Next-Generation Sequencing-Based Spatial Transcriptomics: A Perspective from Barcoding Chemistry

Weixiong Shi,[||] Jing Zhang,[||] Shanqing Huang, Qian Fan, Jiao Cao, Jun Zeng, Lingling Wu,* and Chaoyong Yang*

Cite This: *JACS Au* 2024, 4, 1723−1743

Read Online

ACCESS | Metrics & More | Article Recommendations

ABSTRACT: Gene expression profiling of tissue cells with spatial context is in high demand to reveal cell types, locations, and intercellular or molecular interactions for physiological and pathological studies. With rapid advances in barcoding chemistry and sequencing chemistry, spatially resolved transcriptome (SRT) techniques have emerged to quantify spatial gene expression in tissue samples by correlating transcripts with their spatial locations using diverse strategies. These techniques provide both physical tissue structure and molecular characteristics and are poised to revolutionize many fields, such as developmental biology, neuroscience, oncology, and histopathology. In this context, this Perspective focuses on next-generation sequencing-based SRT methods, particularly highlighting spatial barcoding chemistry. It delves into optically manipulated spatial indexing methods and DNA array-barcoded spatial indexing methods by exploring current advances, challenges, and future development directions in this nascent field.

KEYWORDS: *Spatial transcriptomics, Spatial omics, Next-generation sequencing, Barcoding chemistry, Optical manipulation*
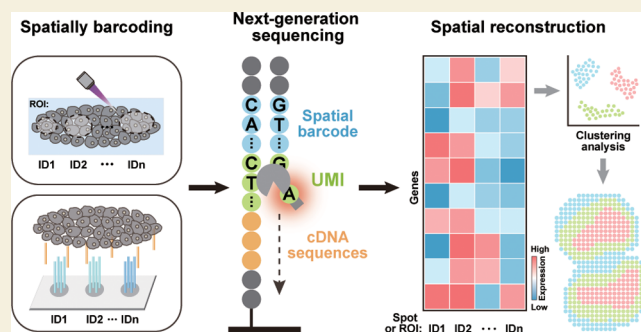
1. INTRODUCTION

In multicellular organisms, cells are organized into complex tissues and organs with intricate spatial patterns to perform diverse physiological functions. Cells do not function in isolation and they proliferate, differentiate, and function while constantly communicating with surrounding cells. For example, embryonic induction occurs widely in developmental biology where cell differentiation is influenced by the surrounding cells.[1] Moreover, tissue function and state are fundamentally tied to the cell type, spatial arrangement, and cell interactions. For example, the composition and distribution of immune cells within the tumor microenvironment determine tumor progression and prognosis.[2] Thus, deciphering the molecular and cellular landscapes is crucial for comprehending a range of biological, physiological, and pathological processes.

Genetic information on cells is stored in the genomic DNA, which is expressed in the transcriptome and the proteome to exhibit distinct phenotypes and functions. With the maturity of next-generation sequencing (NGS), RNA sequencing (RNA-seq) techniques have emerged to measure almost all RNA molecules at unprecedented depth and omics level for revealing gene expression differences and regulatory circuits.[3] Afterward, advancements in microfabrication and cell barcoding techniques have facilitated the development of single-cell

RNA-seq (scRNA-seq), which has revolutionized our ability to define cell types and states.[4,5] Nevertheless, the tissue dissociation in scRNA-seq leads to a loss of spatial context. Therefore, it is highly desirable to measure the RNA characteristics of cells in their native spatial context.

To achieve this aim, spatially resolved transcriptome (SRT) techniques have emerged and come of age over the past few years. They are commonly based on a barcoding chemistry strategy that uses chemical reaction to allocate unique identifiers to target molecules as barcodes for precise spatial and genomic-scale transcript quantitative analyses. Compared with their nonspatial counterparts, a key technical breakthrough of SRT methods is the formation of an accurate connection between the measured transcripts and their derived tissue locations through various physicochemical approaches. With bioinformatics algorithms, transcriptomes from different locations can be reconstructed into a transcriptome atlas of tissues. SRT techniques can provide valuable information on
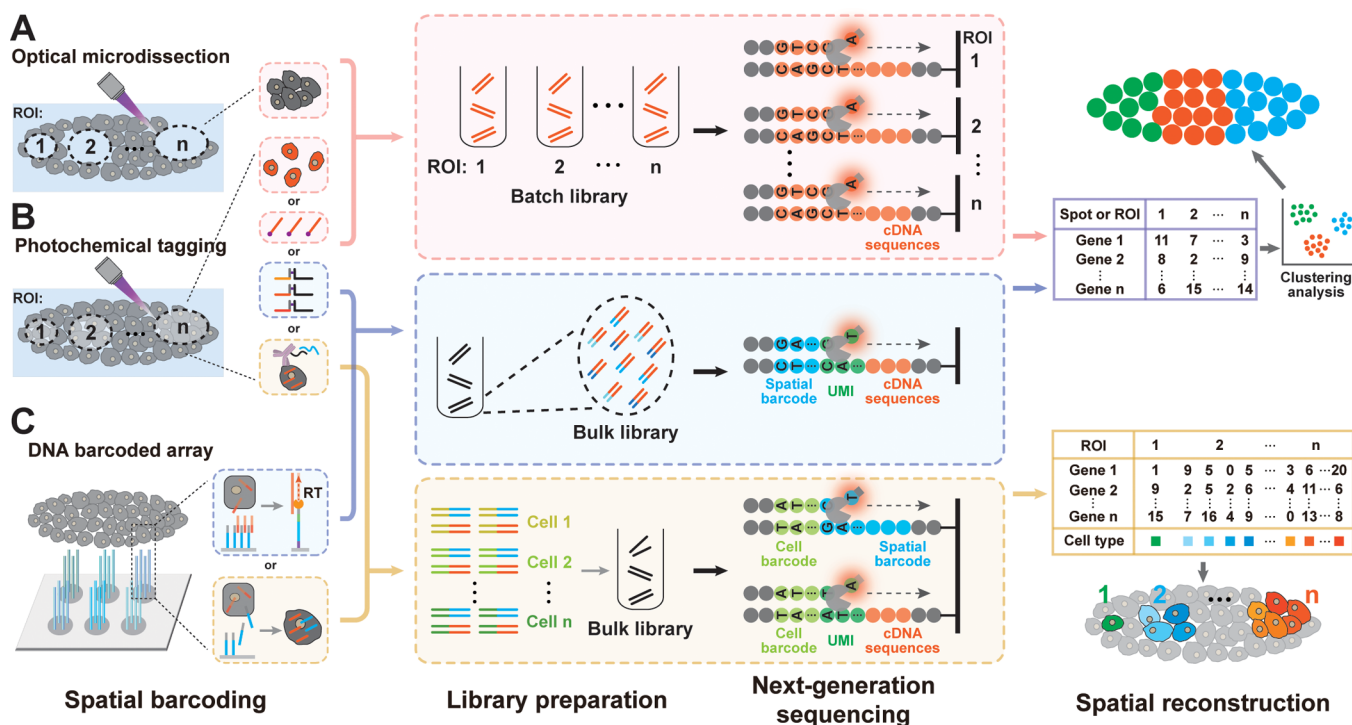
Figure 1. Schematic diagrams for workflows of next-generation sequencing (NGS)-based SRT methods, including spatial barcoding, library preparation, NGS, and spatial reconstruction. (A) Optical microdissection of ROIs followed by batch RNA-seq or batch scRNA-seq for SRT analysis. (B) Photochemical tagging of ROIs to spatially label cells or mRNAs followed by batch scRNA-seq/RNA-seq or bulk RNA-seq for SRT analysis. (C) DNA-barcoded array to spatially barcode cells or mRNAs at whole-tissue level followed by scRNA-seq or bulk RNA-seq for SRT analysis.

Table 1. Main Technical Parameters of ORS Methods

methods	resolution	sensitivity (tissue)[a]	position indexing throughput	detected target	accessibility	ref
Geo-seq	multiple-cell level	~8000 genes/~20 cells (mouse brain)	increasing throughput via multiround LCM	polyA-tailed mRNAs	LCM	22
SPACECAT	multiple-cell level	826 genes/cell (mouse lung tumors)	limited throughput increases via iterative illumination-based color barcoding	polyA-tailed mRNAs	photouncaged tags; Seq-Well	27
ZipSeq	multiple-cell level	3550 genes/cell (3T3 cells)	increasing throughput via iterative illumination-based DNA barcoding	polyA-tailed mRNAs	photouncaged tags; scRNA-seq	29
SCARI	multiple-cell level	NA[b]	limited throughput increases via iterative illumination-based color barcoding	polyA-tailed mRNAs	photosensitive tags; MARS-seq	30
TIVA	single-cell	~10 000 genes/cell (mouse brain)	only one ROI per sample	polyA-tailed mRNAs	photouncaged tags	32
PIC	single-cell/subcellular level	~8000 genes/cell (3T3 cells)	limited throughput increases with iterative illumination	polyA-tailed mRNAs	photouncaged tags; CEL-seq2	26
DSP	1 to ~5000 cells	over 40 types of proteins and 1412 genes/sample (human colorectal tumor)	increasing throughput via iterative illumination	target genes and proteins	photocleavable linker tags	35
Light-Seq	4 to 1000+ cells	10−100 UMIs/μm^2 (mouse retina)	increasing throughput via iterative illumination-based DNA barcoding	whole transcriptome	photocleavable linker tags	36

[a]The units of sensitivity vary according to different methods for more accurate description of sensitivity: "genes/cell" for methods of single-cell resolution, "genes/n cells" for methods of bulk detection of cells in ROIs, and "UMIs/μm^2" for the method of spatial labeling of mRNAs in ROIs. [b]The acronym "NA" stands for "not available."

cell-type compositions, cell locations, and intercellular or molecular interactions. They have empowered novel discoveries in the fields of developmental biology, neuroscience, oncology, and histopathology.

On the basis of different transcriptome measurement methods, current SRT techniques are primarily categorized into imaging-based *in situ* hybridization (ISH)[6−8] or *in situ* sequencing (ISS)[9] and spatial indexing-based NGS.[10] The former utilizes DNA probes to label and encode multiple mRNAs followed by decoding for mRNA quantification and localization via multiround fluorescence imaging, which has been reviewed extensively elsewhere.[11,12] The imaging-based SRT techniques, characterized by single-molecule resolution, offer unparalleled advantages in unveiling the subcellular landscape and uncovering precise intracellular molecular interactions. Despite offering subcellular resolution, these methods require gene-by-gene analysis and primarily rely on targeted probes to measure a predetermined set of genes; thus, they are lengthy and have low throughput. In contrast, the latter SRT methods powered by NGS provide unbiased, genome-level, high-throughput, and cost-efficient analytical solutions. They include two main types of methods according

Table 2. Main Technical Parameters of SBS Methods

methods	resolution (μm)	sensitivity/UMIs per 100 μm² (tissue)[a]	capture area (mm²)	detected target	accessibility[b]	ref
ST	100	31.88 (MOB)[c]	~40	polyA-tailed mRNAs	medium cost; commercialization as 10x Visium	39
10x Visium	55	508 (MOB)	~40	polyA-tailed mRNAs/target genes	high cost; commercially available	76
Ex-ST	~20	~496 (MOB)	~40	polyA-tailed mRNAs	high cost; tissue expansion technique and Visium slides	40
DBiT-Seq	10, 25, 50	~1320−4910 for mRNAs; 121.52 for proteins (ME)[c,d]	25[h]	polyA-tailed mRNAs and ADTs[i]	medium cost; homemade microfluidic chip	64
Decoder-seq	15, 25, 50	4010 (MOB)[e]	25[h]	polyA-tailed mRNAs	low cost; homemade microfluidic chip	63
xDBiT	50	200−800 (mouse organs)	116.64	polyA-tailed mRNAs	medium cost; homemade microfluidic chip	62
RRST	55	173.39 (MB)	~40	target genes	high cost; Visium slides and probe panel design	44
STRS	55	9−36 (mouse heart)[f]	~40	total RNAs	high cost; Visium slides	45
SHM-seq	100	~52 (mouse colon)	~40	host polyA-tailed mRNAs and microbiome rRNAs	high cost; Visium slides	46
SM-Omics	100	13.75 for mRNAs and 1.42 for proteins (MS)[c]	~40	polyA-tailed mRNAs and ADTs[i]	low cost; automated operating systems	41
spatial CITE-seq	25	78.88 for mRNAs; 35.4 for proteins (MS)	6.25	polyA-tailed mRNAs and ADTs[i]	high cost; ADTs and homemade microfluidic chip	53
spatial ATAC−RNA-seq	20, 50[g]	189.36 (ME)	25[h]	open chromatin and polyA-tailed mRNAs	NA; homemade microfluidic chip	49
spatial CUT&Tag−RNA-seq	20, 50[g]	144.12 (P22 MB)	25[h]	polyA-tailed mRNAs and histone modification	NA; homemade microfluidic chip	49
MISAR-seq	50	~450 (ME)	6.25	open chromatin and polyA-tailed mRNAs	NA; homemade microfluidic chip	52
Slide-seq	10	59 (E12.5 ME)	~7	polyA-tailed mRNAs	high cost; spatial decoding	65
Slide-seqV2	10	550 (E12.5 ME)	~7	polyA-tailed mRNAs	high cost; spatial decoding	66
HDST	2	12 (MOB)	13.68	polyA-tailed mRNAs	high cost; spatial decoding	71
Seq-Scope	<1	~1000 (ML)	0.8	polyA-tailed mRNAs	high cost; illumina flow cells	68
Pixel-seq	~1	977 (MOB)	315	polyA-tailed mRNAs	low cost; homemade polony gel	69
Stereo-seq	0.22	1450 (MOB)	up to 132 × 132	polyA-tailed mRNAs	high cost; has been commercialized	67
XYZeq	single cell	1.40 (ML[c]/tumor tissue)	~500	polyA-tailed mRNAs	NA; special facilities for tissue separation	73
sci-Space	single cell	41.23 (E14 ME)	324	polyA-tailed mRNAs	medium cost; sci-RNA-seq	74
Slide-tags	single cell	342.02 (E14 ME)	~7	polyA-tailed mRNAs, open chromatin, and T cell receptors	high cost; droplet-based snRNA-seq	50

[a]UMI counts were obtained from the original publications, and the average UMIs/100 μm² was calculated based on reported feature sizes or bins. [b]Rough cost ranges per sample are defined as follows: high, >$500; medium, $100 to $500; low, <$100. [c]The acronym MOB stands for mouse olfactory bulb, ME for mouse embryo, MS for mouse spleen, MB for mouse brain, and ML for mouse liver. [d]Average UMIs/100 μm² for DBiT-seq of 50 μm resolution. [e]Average UMIs/100 μm² for Decoder-seq of 15 μm resolution. [f]Viral UMIs [mouse heart infected with Type 1-Lang reovirus]. [g]Average UMIs/μm² for spatial ATAC−RNA-seq and spatial CUT&Tag−RNA-seq of 50 μm resolution. [h]Capture area (mm²) for DBiT-seq, Decoder-seq, spatial ATAC−RNA-seq, and spatial CUT&Tag−RNA-seq of 50 μm resolution. [i]The acronym ADTs stands for poly(adenylated) antibody-derived tags.

to difference in spatial barcoding strategies (Figure 1). On the basis of the physical or chemical effects of light, an optically manipulated selection of regions of interest (ROIs) strategy is widely used for spatial indexing, including optical microdissection (Figure 1A) and photochemical tagging (Figure 1B). The isolated cells or extracted mRNA-relative molecules can be detected by batch or bulk scRNA-seq or batch RNA-seq and are further mapped into their corresponding ROIs to generate a tissue spatial atlas. Alternatively, DNA-barcoded array-based SRT techniques enable the spatial barcoding of transcripts or cells at the whole-tissue level with DNA barcodes (Figure 1C). They convert spatial coordinates to sequence barcodes. Both transcripts and position sequences can be read out by NGS for spatial reconstruction of a molecular and cellular landscape of tissues.

This Perspective focuses on NGS-based SRT methods, mainly from the viewpoint of spatial barcoding chemistry. The key detection performances of these methods are summarized and discussed, which encompasses transcript detection sensitivity, spatial resolution, spatial indexing throughput, multiomics feasibility, and accessibility. Transcript detection sensitivity, i.e., detection efficiency, is defined as the percentage of detected transcripts relative to the total existing transcripts for each gene. It is codetermined by the efficiencies of mRNA capture, barcoding, and amplification. Spatial resolution determines the smallest size of a spatially defined region where a higher spatial resolution can delineate a finer tissue atlas. However, this requires spatial barcoding reactions to be executed accurately in micro- or nanometer-scale regions. The position-indexing throughput determines the tissue area to be profiled in a specific period, which is influenced by the multiplex capability of barcoding chemistry. Spatial multiomics allows joint profiling of transcriptome and different omics at the spatial level to reveal regulatory and functional

Table 3. Advantages and Disadvantages Comparison of SBS Strategies

| strategy		advantages	disadvantages
deterministic barcoding	spotting-based barcoding	commercially available spotting instruments for barcoding;	low spatial resolution;
		accessible DNA array slides and kits from commercial 10x Visium;	low detection sensitivity;
		high compatibility with various sample types	high cost of DNA array fabrication
	microfluidics-based barcoding	high flexibility in spatial resolution;	risk of clogging or DNA barcode leakage;
		convenient fabrication DNA arrays only using homemade chip;	limited to single cellular resolution
		relatively high sensitivity	
random barcoding	DNA-barcoded beads	spatial resolution up to 2 μm;	high complexity of barcoded bead synthesis;
		mature bead barcoding method similar to that in scRNA-seq	costly and time-consuming decoding procedure;
			low capture efficiency
	DNA clusters	submicrometer spatial resolution;	costly and time-consuming decoding procedure;
		large capture area;	relying on complex algorithms to determine cell boundaries
		relatively high sensitivity	
scRNA/snRNA-seq assisted spatial barcoding	split-pool based	true single-cell resolution;	time-consuming and tedious procedure to generate barcodes;
		easy generation of unique cell identifiers;	cell/nuclei and mRNA loss during dissociation;
		free of expensive equipment	low spatial resolution of tens to hundreds of microns
	droplet-based	true single-cell resolution;	requiring specialized peripheral equipment;
		one-step cell barcoding;	cell/nuclei loss during dissociation;
		compatible with multiomics	limited to single cellular resolution
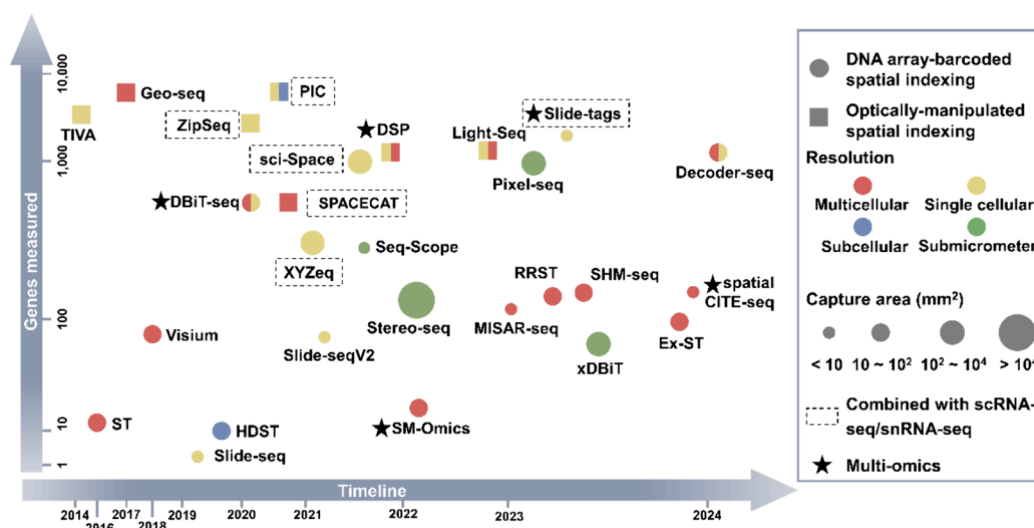
Figure 2. Timeline of the main NGS-based SRT techniques discussed in this Perspective. The *x* axes represent a timeline. The *y* axes represent the number of genes measured per cell (XYZeq, sci-space, Slide-tags, SPACECAT, ZipSeq, TIVA, and PIC) and per sample (Geo-seq and DSP) and the number of unique molecule identifiers per 100 μm^2 (Light-Seq and Pixel-seq) and the number of genes per 100 μm^2 for the other techniques. Squares represent ORS, and circles represent spatially barcoded array-based NGS methods (SBS). Different colors represent different spatial resolution levels. The size of each circle corresponds to the maximum capture area attainable with each SBS method quantified in square millimeters (mm^2). A dashed box denotes those SRT methods combined with scRNA-seq or single-nucleus RNA-seq (snRNA-seq). Black pentagrams highlight spatial multiomics analyses.

mechanisms. Accessibility is mainly determined by the cost and complexity of the experimental operations. Current SRT methods face a trade-off in these detection performances (Tables 1−3 and Figure 2). Finally, current challenges and future development directions are provided for this nascent field.

2. OPTICALLY-MANIPULATED SPATIAL INDEXING METHODS

The most straightforward approach for SRT is to link known spatial locations of isolated ROIs with transcriptomic information. Because of the advantages of high-spatiotemporal resolution and precise directional selection, optically manipulated operations have been widely used to isolate ROIs by physical dissection or photochemical tagging. The isolated ROIs are either combined with bulk RNA-seq or dissociated
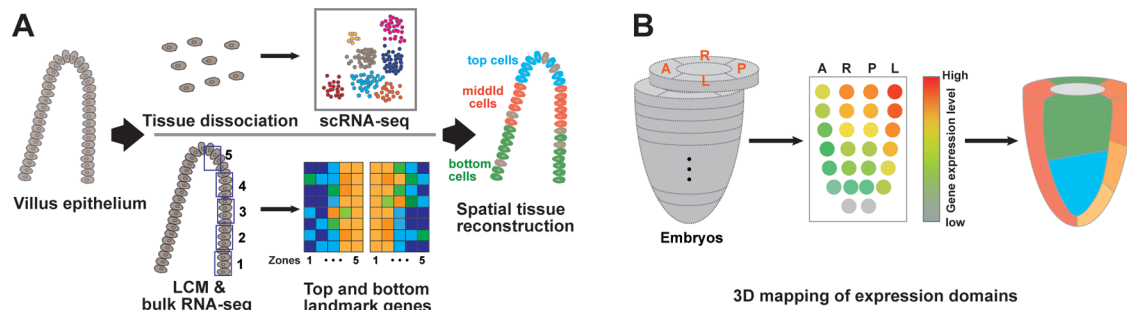
Figure 3. Optical microdissection of ROIs for SRT analysis. (A) Schematic diagram of LCM-RNA-seq integrated with LCM-based bulk RNA sequencing with scRNA-seq for small intestinal villus analysis. Reproduced with permission from ref 20. Copyright 2018 Elsevier. (B) Spatial gene expression in mouse embryos using Geo-seq. Reproduced with permission from ref 23. Copyright 2016 Elsevier.
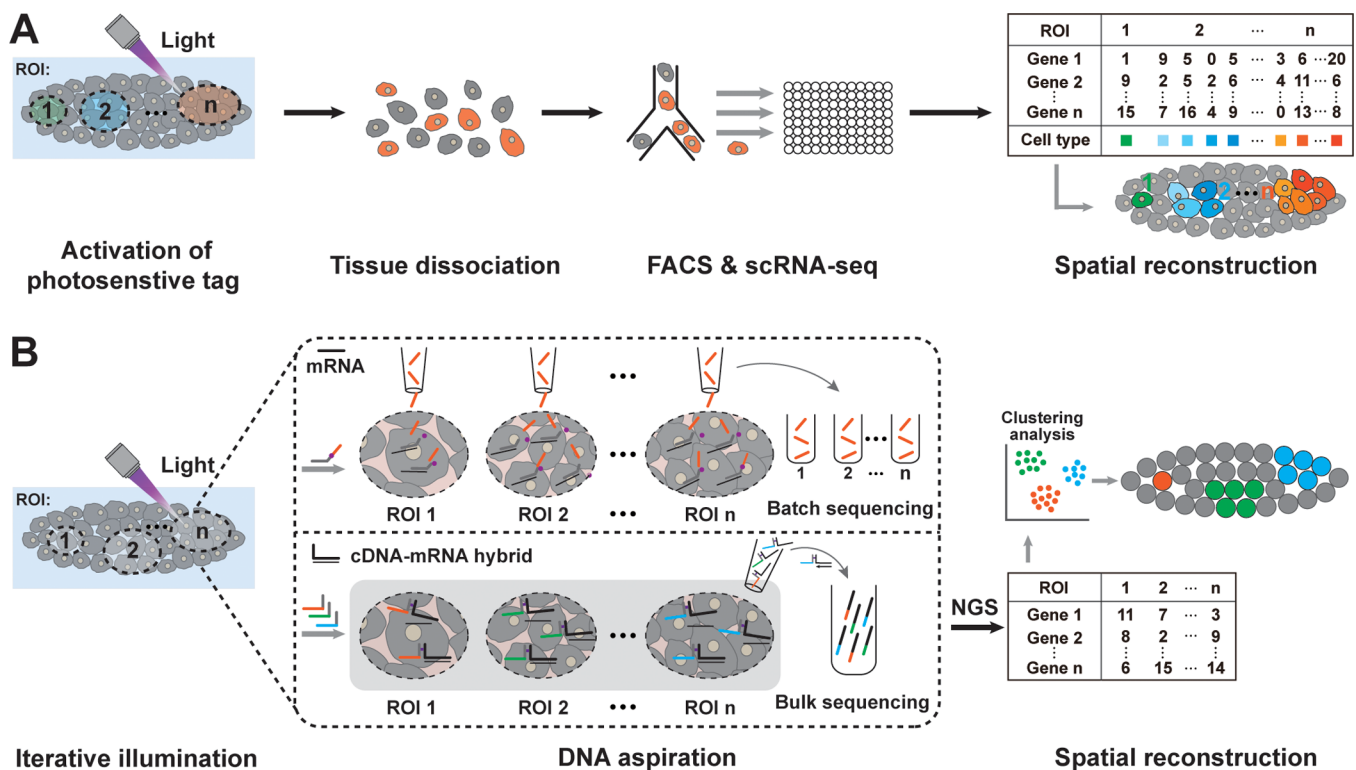

Figure 4. Optical tagging of ROIs for SRT analysis. (A) Schematic diagram of fluoresence labeling of cells in ROIs followed by FACS and scRNA-seq for SRT analysis. (B) Schematic diagram of optical tagging of mRNAs in several ROIs via iterative illumination followed by NGS for SRT analysis.

into single cells for scRNA-seq, thereby allowing for spatial backtracking to obtain the transcriptome and cellular landscape of tissues. With bulk or single-cell RNA-seq, these optically manipulated selections of ROIs for NGS (ORS) methods offer the advantages of high sensitivity and high throughput in gene detection. Nevertheless, they rely on iterative illumination for spatial labeling, which results in a relatively low throughput of spatial indexing. In this section, the existing ORS technologies are summarized with an emphasis on how to enhance the throughput of spatial indexing via photochemical reactions.

2.1. Optical Microdissection of ROIs

Laser capture microdissection (LCM) has emerged as a representative microdissection technology for isolating ROIs from heterogeneous tissues, even at single-cell resolution. ROIs in the tissue section can adhere to the thermoplastic membrane of strong focal adhesion by near-infrared laser or can be dissected using high-energy ultraviolet (UV) light under a

microscope.[13−15] The isolated cells or cell clusters are lysed for RNA sequencing to correlate the transcriptome with ROI positions. Early studies required hundreds to thousands of isolated cells to provide sufficient amounts of RNAs, thus limiting spatial resolution.[16,17] By integrating highly sensitive scRNA-seq techniques, called Smart-seq2,[18] Nichterwitz et al. developed laser capture microscopy coupled with full-length mRNA sequencing (LCM-seq) for single-cell transcriptomics (Figure 1A).[19] Through direct cell lysis instead of the original RNA extraction using RNA isolation kits, LCM-seq improved the cDNA yield to achieve a 62% success rate for single-cell analysis. Thus, LCM-seq demonstrated the ability to analyze the transcriptome of a single neuron in mouse and human tissues and revealed that the transcription factors *Pbx3* and *Nfib* not previously implicated in motor neuron function were differentially expressed along the spinal cord. However, this method was low-throughput and provided inaccurate spatial
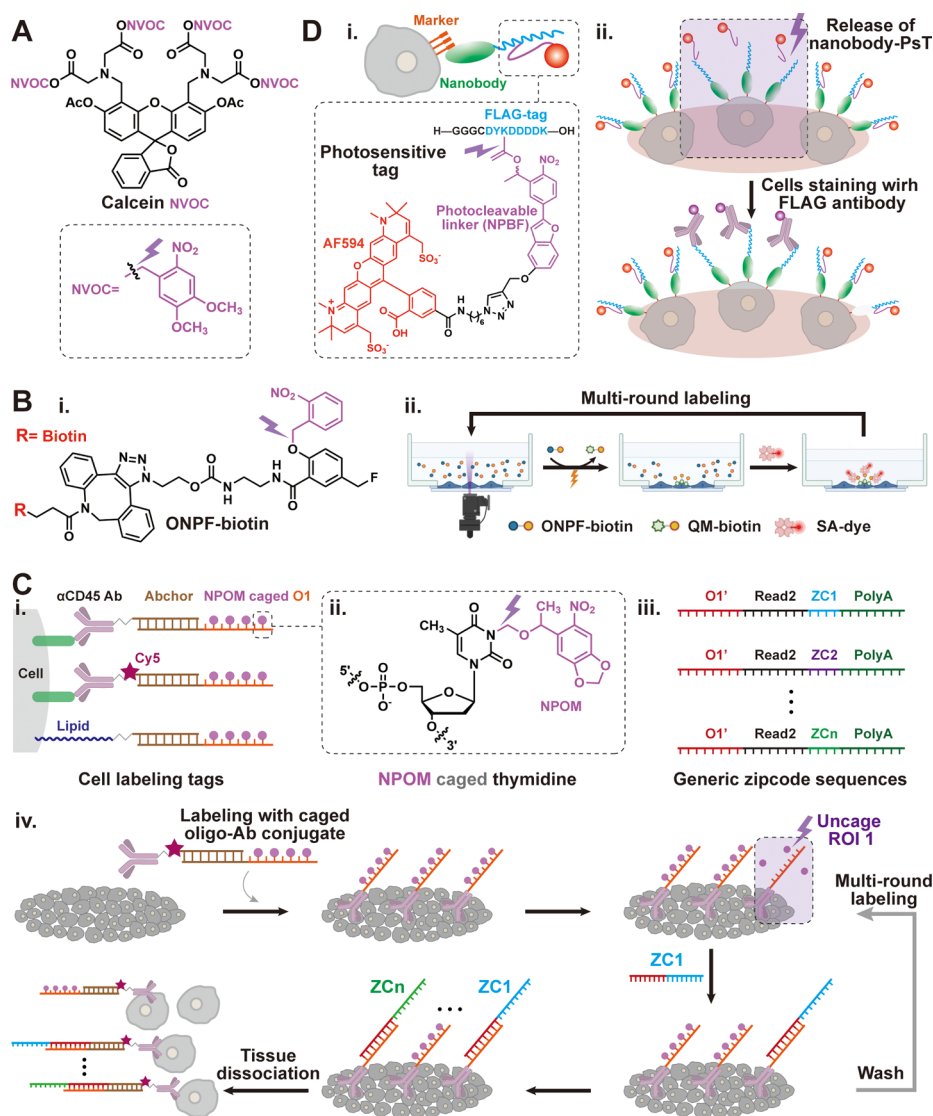
Figure 5. Fluorescence labeling of cells for SRT analysis. (A) Structural formula of calcein NVOC (top) and NVOC (bottom) in SPACECAT. (B) Structural formula of ONPF-biotin (i) and schematic diagram of fluorescent labeling of multiple ROIs in OpTAG-seq (ii). Reproduced with permission from ref 28. Copyright 2021 John Wiley and Sons. (C) Schematic diagram of cell labeling with zipcode tags (i), zipcode sequences (iii), and multiple ROI labeling (iv) and structural formula of NPOM-caged thymidine (ii) in ZipSeq. (D) Schematic diagram of cell labeling with a photosensitive tag (its structural formula is in the dashed box) (i) and signal switch system for selective single-cell analysis (ii) in SCARI.

reconstruction of whole tissue sections because of the unsatisfactory success rate in single-cell analysis and the labor-intensive process of manually isolating numerous individual cells. To overcome this challenge, Moor et al. developed RNA sequencing of laser capture microdissected tissue (LCM-RNA-seq), which conducted bulk RNA sequencing of specific ROIs to define a set of zonated landmark genes (Figure 3A).[20] The landmark genes could be utilized to reconstruct the spatial tissue coordinates of single cells in the scRNA-seq data. LCM-RNA-seq revealed extensive partitioning of the enterocyte function along the villus axis. Similarly, Baccin et al. employed a similar strategy to assign cell types to distinct ecological niches within mouse bone marrow, thereby uncovering their molecular, cellular, and spatial compositions.[21]

Three-dimensional (3D) SRT analysis can depict the molecular and cellular landscapes of whole tissues within their natural spatial contexts, thereby facilitating the study of physiological and pathological processes. Jing's group

developed geographical position sequencing (Geo-seq) for spatial transcriptome profiling of the entire early mouse embryo (Figure 3B).[22−24] Geo-seq was conducted by performing low-input RNA-seq on individual ROIs isolated with defined positions by LCM in a 3D manner. Specifically, embryos were serially cryo-sectioned, and each section was sampled from four quadrants with approximately 20 epiblast cells per ROI. After sequencing and digital 3D reconstruction, Geo-seq achieved a genome-wide molecular architecture of lineage allocation and tissue organization in early mouse embryo.[23,24]

LCM is a powerful and accessible technique for dissecting ROIs and even single cells using many commercialized instruments. Combined with bulk RNA-seq and scRNA-seq, LCM enables high-throughput and high-sensitivity transcriptome detection. Nevertheless, these methods have limited throughput of spatial indexing as they rely on repeated LCM and batch sequencing, which is impractical for large tissue analysis. Laser irradiation inevitably causes damage to the

sample. In addition, it is difficult for LCM to achieve a subcellular resolution.

2.2. Photochemical Tagging of ROIs

Photochemical tagging is a novel strategy for precise spatial annotation of cells or molecules in ROIs by photochemical reactions with spatial resolution up to the diffraction limit for SRT compared with LCM. Specifically, tissue cells or mRNAs are commonly labeled with photosensitive tags containing photolabile *o*-nitrobenzyl-based chromophores, such as 6-nitropiperonyloxymethyl (NPOM), 6-nitroveratryloxycarbonyl (NVOC), or 4-nitrophenyl(benzofuran) (NPBF), or containing photo-cross-linker. Photosensitive tags undergo reactions of uncaging, cleaving, and cross-linking under light illumination in ROIs for position marking. SRT methods based on the optical marking of ROIs can be classified into two main groups: (1) spatial labeling of cells with fluorescence in ROIs, followed by tissue dissociation, cell isolation via the fluorescent-activated cell sorting method (FACS), and scRNA-seq analysis (Figure 4A), and (2) spatial tagging of mRNA in ROIs for physical aspiration and bulk RNA-seq (Figure 4B). Much effort is devoted to improving the sensitivity, spatial barcoding throughput, and isolation selectivity.

2.2.1. Fluorescence Labeling of Cells in ROIs.
Various photosensitive tags, including photoactivatable fluorescent tags and photouncaged tags, have been designed and synthesized for the fluorescence labeling of cells in ROIs via light illumination followed by FACS-based target cell isolation. By combination with scRNA-seq, this methodology can achieve high detection sensitivity and contribute to accurate cell type and function analysis, such as the identification of rare immune cell subgroups and detection of state changes under viral infection. For example, with photoactivatable green fluorescent protein (PA-GFP) tags and two-photon laser microscopy, Amit's group developed NICHE-seq for spatial reconstruction of immune niches.[25] Transgenic mice expressing PA-GFP were used for *in situ* spatial labeling of cellular niches by activating the GFP fluorescence. The labeled cells were analyzed by massively parallel scRNA-seq (MARS-seq).[26] NICHE-seq was capable of analyzing thousands of cells in the specific niches of the lymph nodes and spleen of mouse after viral infection, thereby elucidating the assembly of high-order functional units in multicellular organisms through immune cell networks. However, genetic models require labor-intensive genetic modification and are not applicable to human tissues. Genshaft et al. introduced photolabile NVOC to cage carboxylate groups of calcein, a commonly used cell viability dye, which enabled arbitrary labeling of live cells by photouncaging reaction for tracking and isolation (Figure 5A).[27] With calcein NVOC, they developed a method, termed Spatially Photoactivatable Color Encoded Cellular Address Tags (SPACECAT), to label and isolate cells in user-defined positions for scRNA-seq. The activated fluorescence of labeled cells maintained temporal stability (>16 h), which allowed subsequent cell dissociation and FACS. This method was applicable to almost all types of live tissue samples and only required immersion in calcein NVOC containing media. Two additional photocaged dyes were synthesized to increase the multiplex capability of spatial barcoding but they suffered from complex probe design and synthesis.

To achieve convenient multiplex ROI labeling, Chen's group developed a general optical cell tagging (OpTAG) strategy and thus established OpTAG-seq by synthesizing photosensitive ONPF-biotin, which was produced by reacting an azide-functionalized photoactivatable quinone methide (AzONPF) with aza-dibenzocyclooctyne-conjugated biotin (DBCO-biotin) (Figure 5B-i).[28] ONPF-biotin contained three important moieties: (1) a photosensitive *o*-nitrobenzyl group for caging, (2) a quinone methide (QM) to react with amines and thiols of proteins on cell surfaces via Michael addition, and (3) a biotin that reacted with streptavidin-modified dyes (SA-dyes). Under UV illumination, ONPF-biotin was converted to QM-biotin for covalently tagging adjacent cells, which were further labeled with SA-dyes for FACS and scRNA-seq. Marking of different ROIs was readily achieved through multiround UV illumination and different SA-dye labeling (Figure 5B-ii). Thus, OpTAG-seq would be useful for studying the spatiotemporal regulation of gene expression in various multicellular systems. Nevertheless, the color barcoding strategy had limited multiplex capacity, and cells in different ROIs had to undergo separate scRNA-seq. To overcome this challenge, Krummel's group developed ZipSeq by serially light printing DNA barcodes as zipcodes (ZC) onto the surface of cells to barcode multiple ROIs for spatially defined scRNA-seq (Figure 5C).[29] Double-stranded "anchor strands" with antibody or lipid modification were used for selective or universal cell labeling, and their overhang sequences (termed "O1") were photocaged at four sites using NPOM conjugated to thymidine (Figure 5C-i,ii). Only under UV illumination could the uncaged O1 be hybridized with "ZC" strands, which contained sequences (5′ to 3′) of complementary O1 (O1′), illumina Read2, ZC, and polyadenylated (polyA) tail for cell labeling, sequencing, ROI barcoding, and polydeoxythymidine (polyT)-based amplification, respectively (Figure 5C-iii). Thus, ZC strands tagged on the cell surface could be sequenced, along with mRNAs, during scRNA-seq for SRT analysis (Figure 5C-iv). ZipSeq enabled multiplex ROI labeling with multiround illumination for simultaneous scRNA-seq, and multiplex capability could be theoretically scaled up through the design of orthogonal overhang sequences or barcoded polyA strands. In ZipSeq, the new gene expression patterns associated with histological structures were discovered in *in vitro* wound healing, live lymph node sections, and a live tumor microenvironment, which revealed how cellular transcriptional heterogeneity was affected by the local environment.

To improve selectivity of isolating uncaged cells due to the common occurrence of ambiguous cells in the above-mentioned photouncaging strategies, van der Leun et al. developed a photocage-based signal switch system for single-cell analysis of ROIs (SCARI, Figure 5D).[30] They synthesized a photosensitive tag (PsT) containing a FLAG peptide, which was protected by an Alexa Fluor 594 (AF594)-conjugated photolabile NPBF (Figure 5D-i). After photouncaging, the AF594 dye was released, and the exposed FLAG tag allowed attachment of fluorescent FLAG antibody (Figure 5D-ii). Only the simultaneous first signal loss and second signal gain could be determined as a photouncaged reaction, thereby accurately distinguishing uncaged and caged cells. Moreover, with PsT-labeled nanobodies, target cells, including rare cell types, could be marked by signal switch at a defined ROI for in-depth scRNA-seq.[31] In addition, NPBF possessed superior uncaging efficiency under low-intensity UV light with a low photo-toxicity. SCARI was capable of spatially resolving live cells isolated from ROIs in complex *in vitro* systems.
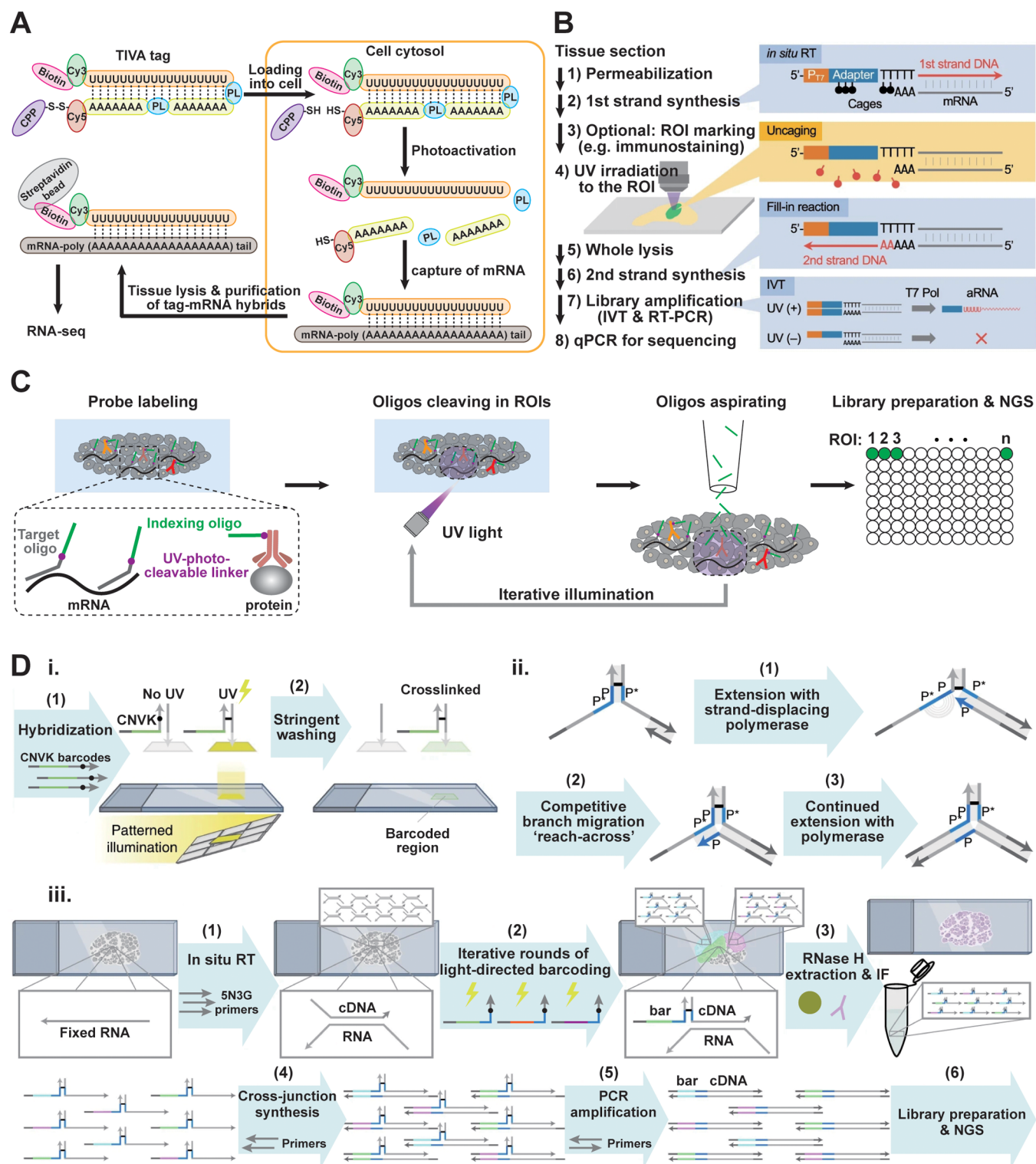
Figure 6. Spatial tagging of mRNAs in ROIs for SRT analysis. (A) Schematic diagram of TIVA. (B) Schematic diagram of a transcriptome profiling method coupled with photoisolation chemistry. Reproduced with permission from ref 33. Copyright 2021 Springer Nature. (C) Workflow of DSP. (D) Schematic diagram of Light-Seq, including photo-cross-linking barcoding chemistry (i), cross-junction synthesis reaction (ii), and DNA barcoding of cDNAs in multiple ROIs (iii). Reproduced with permission from ref 36. Copyright 2022 Springer Nature.

These strategies of fluorescence labeling of cells in ROIs can be easily combined with mature scRNA-seq workflows for SRT to offer the advantages of high-transcript-detection sensitivity. Moreover, no cell fixation is required, which enables real-time marking of ROIs in live tissues for time-resolved SRT. With photosensitive tag-labeled recognition molecules, rare cells that

are commonly missed by other SRT methods can be specifically labeled and isolated for scRNA-seq. Nevertheless, the throughput of spatial barcoding is still unsatisfactory, which poses challenges for the SRT of whole tissues. In addition, some cells may be lost because of multiple operation steps and limited cell utilization during scRNA-seq.[31] Furthermore, these
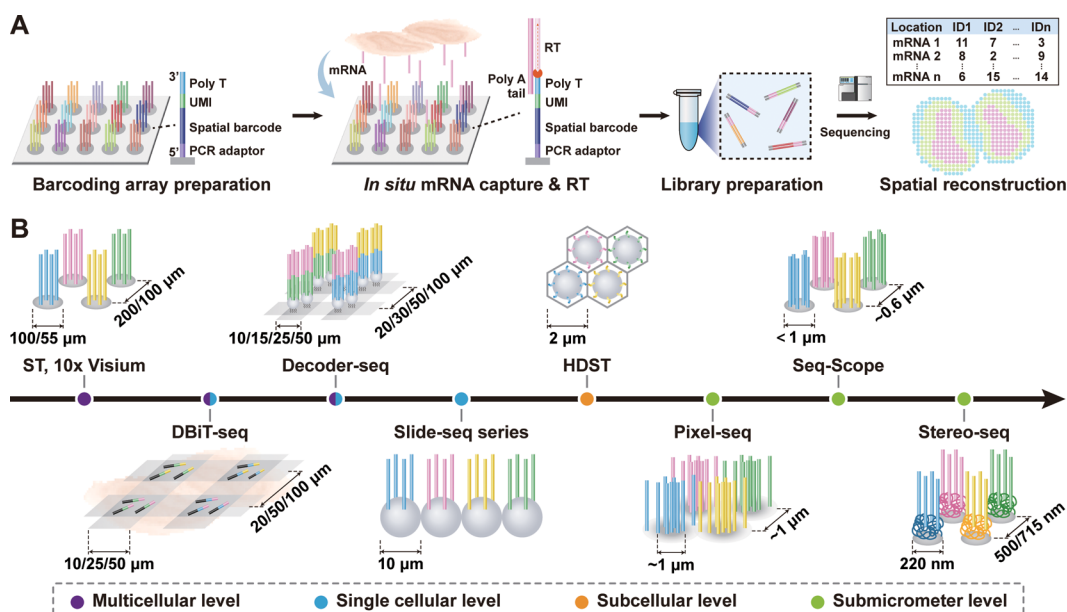
Figure 7. SBS methods for SRT analysis. (A) Schematic diagram of SBS for spatial transcriptome analysis. (B) Summary of the spatial resolution of landmark SBS techniques.

SRT methods are incompatible with tissues that exhibit difficulties in single-cell dissociation.

2.2.2. Spatial Tagging of mRNAs in ROIs. The strategies of spatial labeling of mRNAs in ROIs are more applicable to various tissue samples, such as frozen and archived tissues, whose multiplexed spatial indexing can be achieved by iterative illumination and target molecule extraction instead of single-cell sorting after labeling (Figure 4B). Lovatt et al. engineered a multifunctional photoactivatable mRNA capture molecule for transcriptome in vivo analysis (TIVA) of spatially defined single cells in live tissues (Figure 6A).[32] The TIVA tags consisted of four functional moieties: (1) disulfide-linked cell-penetrating peptide (CPP) to transport tags into cells, (2) Cy3-Cy5 pair to visualize uncaging and label cells via fluorescence resonance energy transfer signal, (3) mRNA-capturing moiety, and (4) biotin to capture and purify TIVA tag-mRNA hybrids. The mRNA-capturing moiety was designed as a photocaged hairpin oligo containing photo-cleavable linkers, which could expose poly (2′-deoxy-2′-fluorouridine) capture oligos under UV illumination to bind the polyA tail of mRNAs. After aspirating and purifying tag-mRNA hybrids, RNA-seq revealed that single neurons expressed ~12 000 and ~5000 genes, respectively, in live mouse and human brain tissue, and their transcriptomic landscapes were shaped by tissue microenvironment. However, TIVA was applicable only to live tissue and was incompatible with histological characterization for selective single-cell analysis. For spatial transcriptome analysis of fixed tissues with high resolution, Honda et al. developed a transcriptome profiling method coupled with photoisolation chemistry (PIC, Figure 6B).[33] Photocaged oligodeoxynucleotides (caged ODNs) were used for primers for in situ reverse transcription (RT), which contained several 6-nitropiperonyloxymethyl deoxythymidines (NPOM-dTs) to suppress the read-through of DNA polymerase I. After photouncaging, second-strand synthesis could be activated. Using immunostaining to define ROIs for spatial uncaging, cDNA-mRNA hybrids could be extracted for RNA-seq following CEL-seq2 (cell expression by

linear amplification and sequencing).[34] PIC with high sensitivity enabled the detection of ~8000 genes per cell and 28.5−80.3 unique molecule identifiers (UMIs) per μm^2. Using digital mirror devices (DMDs), PIC achieved transcriptome analysis of subcellular and subnuclear microstructure.

To achieve multiplex spatial labeling of omics molecules in different ROIs, Merritt et al. developed a digital spatial profiling (DSP) system capable of spatial multiplex analysis of both transcriptome and proteins for tissue samples (Figure 6C).[35] Photocleavable tags were designed with three important moieties: (1) a unique indexing oligo for protein or RNA quantification, (2) an affinity reagent (antibody or mRNA probe) for protein or mRNA labeling, and (3) a photo-cleavable linker to release the spatially resolved unique indexing oligos. With programmable a DMD and iterative illumination, the indexing oligo panels were sequentially released in different ROIs and then collected via microcapillary aspiration for separate sequencing to readout proteins and mRNAs. DSP was capable of single-cell resolution. With NGS, analysis throughput of mRNA could achieve 1412 genes. However, DSP relied on designing numerous targeted mRNA probes and required separate sequencing libraries for distinct ROIs, which made it incompatible with unknown gene profiling and high-throughput spatial barcoding. To solve this problem, Yin's group developed light-directed DNA barcoding of cDNAs in fixed cells and tissues for multiplexed spatial indexing sequencing (Light-Seq, Figure 6D).[36] Light-Seq involved a light-controlled DNA barcode attachment strategy by combining photo-cross-linking barcoding chemistry (Figure 6D-i) and cross-junction synthesis reaction (Figure 6D-ii).[37] Barcode strands containing an ultrafast photo-cross-linker, 3-cyanovinylcarbazole nucleoside (CNVK), could photo-cross-link to a pyrimidine base in a complementary sequence after a short UV illumination.[38] RT primers were designed to contain five N and three G bases on the 3′ end and a barcode docking site on the 5′ end for in situ RT of the tissue whole transcriptome regardless of polyadenylation. CNVK- and UMI-containing barcode strands were iteratively hybridized and
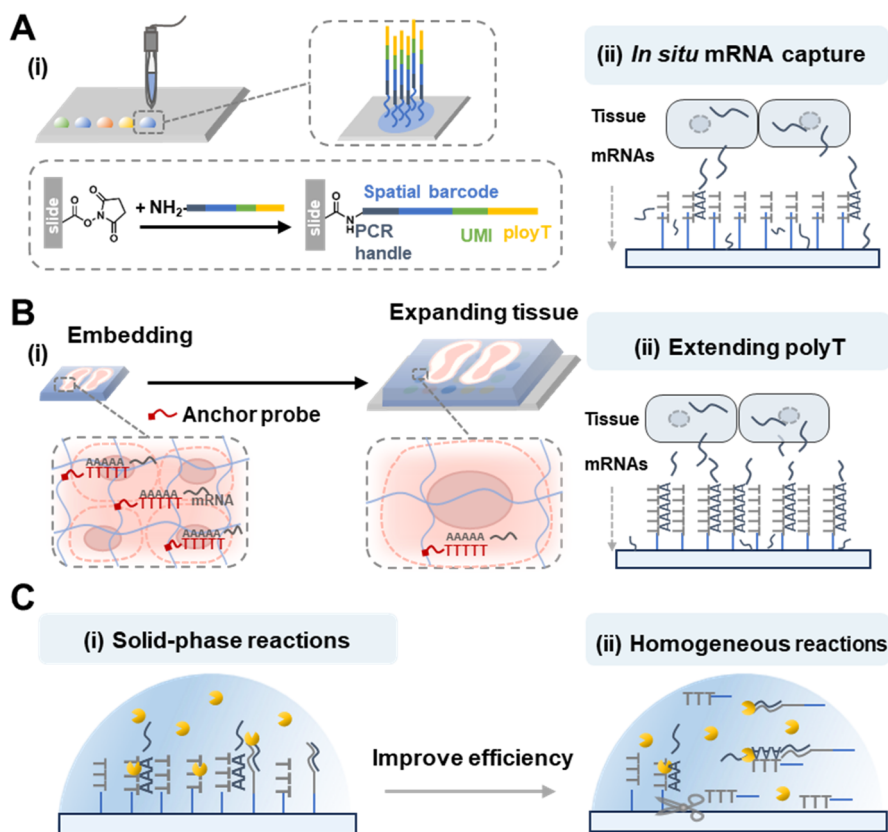
Figure 8. Spotting-based barcoding strategies for SRT analysis. (A) Schematic diagram of barcoded array preparation using a microarrayer spotting robot (i) and *in situ* capture of residual mRNAs (ii) in ST and 10x Visium. (B) Schematic diagram of increasing resolution using tissue expansion (i) and increasing capture efficiency of mRNAs in Ex-ST. (C) Schematic diagram of RT reaction at solid-liquid interface in ST (i) and homogeneous RT reaction in SM-Omics by releasing mRNA primers from substrate for (ii).

photo-cross-linked to the 5′ docking site on all cDNAs in multiple ROIs. With RNase H treatment, cross-linked strands of barcoded strands and cDNA were simultaneously extracted and further stitched together using a cross-junction synthesis reaction to create pooled, spatially indexed sequencing libraries (Figure 6D-iii). Light-Seq yielded 1000−10 000 UMIs detected per 10×10 μm^2, with mean gene sensitivity of $4.29 \pm 3.39\%$, which is in line with existing sequencing-based SRT methods. More importantly, the joint analysis of morphology, tissue context, transcriptome, and protein expression in the same cells offered a more comprehensive measurement of cell state and interactions. Meanwhile, Light-Seq enabled rare cell transcriptomics analysis and identified biomarkers for a very rare neuronal subtype in mouse retinal sections for the first time.

These strategies of spatial tagging of mRNAs in ROIs avoid tedious and time-consuming procedures, as well as cell loss during tissue dissociation, cell isolation, and scRNA-seq. These methods are compatible with a wider range of tissue types, especially when target cells are rare or difficult to isolate. They provide an accessible workflow to combine *in situ* imaging and protein staining with NGS for selective analysis of multiple cells or regions of interest. Moreover, most of these methods retained tissue intact, which allowed reuse of tissue sections for further experimental analyses.[35,36] Nevertheless, the accuracy of spatial barcoding is limited, probably because of diffusion of RNAs or cDNAs and light-scattering-induced out-of-ROI barcoding. In addition, barcoding using tedious iterative illumination is still impractical for whole tissue SRT. Moreover,

the detection sensitivity of mRNAs is affected by efficiencies of multistep reactions, such as intercellular mRNA capture and photoactivated reaction.

3. DNA ARRAY-BARCODED SPATIAL INDEXING METHODS

DNA sequences can be employed as spatial barcodes to tag tissue mRNAs or cells and read out with high-throughput NGS. This innovative concept is similar to high-throughput scRNA-seq where mRNAs of individual cells are labeled with unique DNA barcodes before bulk library preparation for NGS. Building upon this, spatially barcoded array-based NGS methods (SBS) have been developed for SRT (Figure 7A). Typically, DNA-barcoded arrays are first fabricated with thousands of pixels. Each pixel contains unique barcoded DNA primers for unbiased capture of mRNAs. The barcoded oligos commonly consist of (5′ to 3′) (1) a PCR adaptor for downstream PCR and sequencing reaction, (2) a spatial barcode for location indexing of each position, (3) a UMI to correct amplification bias and quantify mRNAs, and (4) a polyT sequence for unbiased capture of polyA-tailed mRNAs. Then, a thin tissue section of about a monolayer of cells is placed on the arrayed surface and permeabilized for mRNA or cell labeling by barcoded oligos. After RT, library preparation, and NGS, DNA sequences containing transcript information and/or spatial barcodes are read out for SRT mapping (Figure 7A). SBS technologies integrate the merits of interfacial barcoding chemistry and sequencing chemistry to achieve
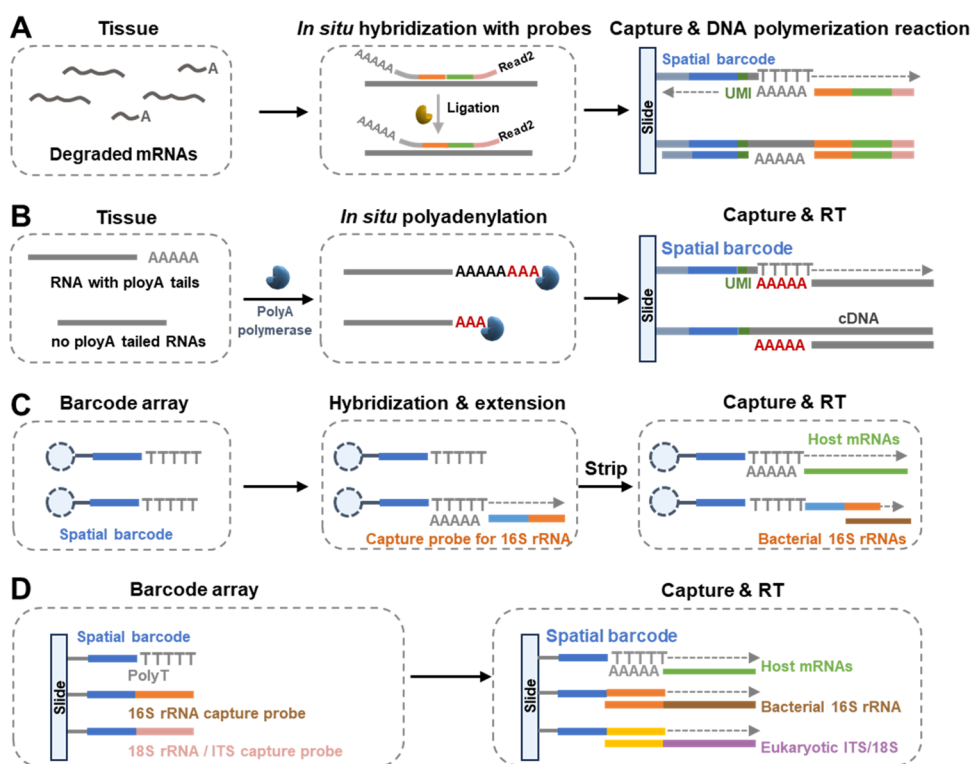
Figure 9. Strategies of capturing and spatially barcoding RNAs without polyA tails for SRT analysis. (A) Schematic diagram of capturing protein-coding regions of degraded and fragmented mRNAs using a probe-pair-based ligation reaction in RRST. (B) Schematic diagram of *in situ* polyadenylation and capture of the total RNAs in STRS. (C) Schematic diagram of conjugating 16S rRNA probes for capturing host mRNAs and bacterial 16S rRNAs at the same time in SHM-seq. (D) Schematic diagram of conjugating three types of capture probes for capturing bacterial and fungal rRNAs, as well as host mRNAs at the same time in SmT.

straightforward, transcriptome-wide, and high-throughput SRT profiling.

The spatial resolution of SRT is critically determined by the pixel size of DNA-barcoded arrays, and remarkable methodologies have been developed to fabricate finer arrays with smaller pixels. These technologies have enhanced the resolution from a multicellular level (100 μm) to a single-cell (10 μm) and subcellular level (2 μm) and further up to a submicrometer level ($\sim$220 nm) (Figure 7B). According to different spatial barcoding strategies, SBS approaches are primarily classified into three types: deterministic barcoding, random barcoding, and barcoding assisted by scRNA-seq or snRNA-seq. In this section, we will summarize these three types of SBS methods with an emphasis on how to enhance resolution and sensitivity and correlate multiomics from the perspective of barcoding chemistry.

3.1. Deterministic Barcoding Strategies

Deterministic barcoding strategies harness microarrayer spotting robots or microfluidic chips to deposit deterministic barcoded oligomers at specific positions on substrates. The barcoded substrates are ready for SRT analysis without the requirement of time-consuming decoding for position indexing.

3.1.1. Spotting-Based Barcoding. In 2016, Ståhl et al. developed spatial transcriptomics (ST), which is the first SBS method.[39] A microarrayer spotting robot was used to deposit 5′-amino-modified polyT oligos on *N*-hydroxysuccinimide-functionalized glass slides for covalent conjugation (Figure 8A-i). The resulting spatially barcoded array contained 1007 spots, each with the diameter of 100 μm and a center-to-center

distance of 200 μm, which covered a barcoded area of 6.2 mm × 6.6 mm. The density of conjugated oligomers was $\sim$200 million per spot. After tissue permeabilization and mRNA release and capture (Figure 8A-ii), ST achieved 6.9 $\pm$ 1.5% detection sensitivity compared with single-molecule ISH. On the basis of ST, 10x Genomics has released Visium Spatial Gene Expression Solution (known as 10x Visium), which reduced spot diameter and center-to-center distance to 55 and 100 μm, respectively (Figure 7B). By offering commercially available slides, kits, and procedures, 10x Visium expands the application scope of the SRT technique to neuroscience, cancer biology, and developmental biology. Nevertheless, spots with diameters of 100 or 55 μm are occupied by several to dozens of cells, which is far from achieving the goal of single-cell resolution for SRT analysis.

The generation of barcoded spots with sizes approaching single-cell diameter using a microarrayer spotting method is challenging because of factors such as droplet evaporation and merging, as well as instrumental accuracy. Instead of shrinking spot size, Wang's group developed expansion spatial transcriptomics (Ex-ST) by linking tissue sections covalently to swellable polyelectrolyte hydrogel for physical expansion before the 10x Visium procedure (Figure 8B-i).[40] Two types of polyT probes of different lengths were designed for mRNA anchoring and spatial barcoding. The shorter ones with a melting temperature of $\sim$39 °C had 5′-acrydite modification for mRNA anchoring in a polyacrylate gel. The longer ones, with a melting temperature of >55 °C, were conjugated on the 10x Visium array slides. After digesting protein, the mRNA-anchored gel underwent $\sim$2.5-fold linear expansion in buffer. The mRNAs were then released from the gel by heating and
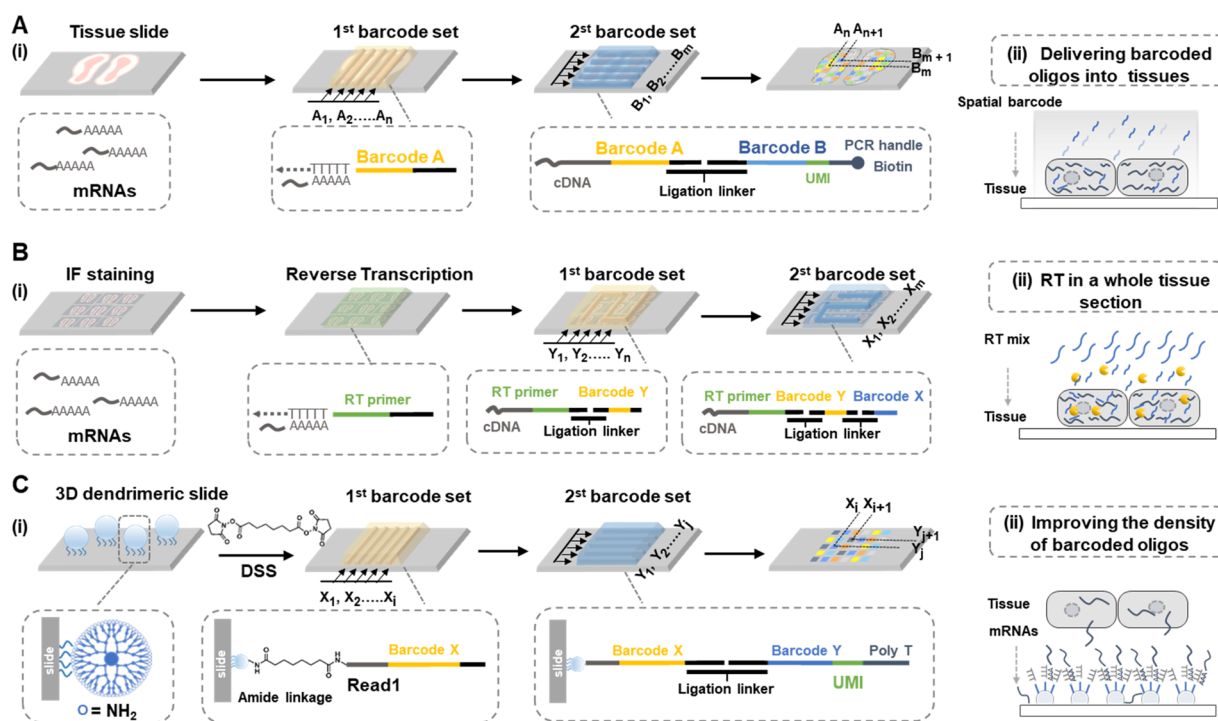
Figure 10. Microfluidics-based barcoding strategies for SRT analysis. (A) Schematic diagram of microfluidics-based combinatorial barcoding of tissue mRNAs (i) and delivering barcoded oligos into permeabilized tissues (ii) in DBiT-seq. (B) Schematic diagram of multiplexed deterministic barcoding in tissue using serpentine microchannel chips (i) and RT in a whole tissue section instead of RT in the microchannel to improve RT efficiency (ii) in xDBiT. (C) Schematic diagram of preassembling barcoded DNA array on 3D dendrimer substrates using microfluidics-based combinatorial barcoding strategy (i) and enhanced oligo density for efficient mRNA capture (ii) in Decoder-seq.

captured on array slides, followed by standard SBS-based SRT protocol. This tissue expansion strategy successfully extended the spatial resolution of the Visium array from 55 μm to ~20 μm. Most spots had occupancy by a single cell type of >80% for mouse hippocampus tissue sample. Moreover, Ex-ST adopted barcoded primers of 50 thymidine instead of the standard 30 thymidine in 10x Visium (Figure 8B-ii). This also extended the time of RT to enhance efficiency and used a higher concentration of beads during the cleanup step to retain more fragments. With these modified operations, Ex-ST captured 35% more UMIs than 10x Visium. With enhanced resolution and sensitivity, Ex-ST successfully identified glomeruli in mouse olfactory bulbs (MOBs) and uncovered the subcellular distribution of neuron transcripts.

In light of the low efficiency of RT reaction in solid–liquid interface during ST (Figure 8C-i), in the spatial multi-omics (SM-Omics) method, barcoded primers, as well as their captured mRNAs, were released from the substrate for more efficient homogeneous RT reaction (Figure 8C-ii).[41] Meanwhile, the researchers optimized the amount of sequencing adapters and reaction time to improve the efficiency of library preparation reactions in SM-Omics. These optimizations contributed to 3.2-fold increase of genes and 3.6-fold higher UMI detection in SM-Omics compared with those in ST. In addition, DNA-barcoded antibodies were used as tags to label target proteins, and SM-Omics enabled simultaneous capture and spatial barcoding of mRNAs and protein tags, thereby achieving spatial transcriptomics and spatial multiplex protein detection. Similarly, Landau's group developed Spatial PrOtein and Transcriptome Sequencing (SPOTS) for high-throughput simultaneous spatial transcriptomics and >30 protein profiling using the polyA capture technology of the Visium slide.[42] This

multimodal approach yielded superior tissue mapping of cell types, biological processes, and phenotypes.

The classical 3′-polyA capture strategy would miss degraded and fragmented mRNAs without polyA tails, which would reduce the detection sensitivity for easily degraded tissues and formalin-fixed paraffin-embedded (FFPE) samples. In addition, some samples are difficult to efficiently permeabilize for mRNA release, and some precious clinical samples with limited amount are not sufficient for permeabilization optimization and RNA quality assessment. To solve these challenges, a gene panel probe capture strategy was developed for capturing protein-coding regions of the transcriptome instead of the polyA tails, which was less dependent on the RNA integrity. Visium spatial gene expression for FFPE of 10x Genomics[43] and RNA-Rescue Spatial Transcriptomics (RRST, Figure 9A)[44] were two representative methods. Generally, sections of FFPE tissues or formalin-fixed tissues are permeabilized and incubated with probe sets, which were designed to label about 19 000 protein-coding genes. Each transcript was labeled with at least a pair of probes, and only the probe pair simultaneously hybridized with target transcript to trigger a ligation reaction for generating intact sequences of 3′-polyA and 5′-primer. After tissue digestion, the released probes were captured on a barcoded array for cDNA synthesis, library preparation, and sequencing. Theoretically, this strategy could improve the recovery of mRNAs with moderate-to-low RNA quality, thus significantly improving gene detection sensitivity. For example, RRST could profile a transcriptome of tissues of different qualities and origins with 2-fold to 100-fold increase in the number of detected genes per spot compared with the standard polyA mRNA capture strategy.[44] This expanded the application scope of SRT to challenging tissue types, including

human lung, colon, small intestine, pediatric brain tumor, and mouse bone/cartilage. Nevertheless, this targeted capture strategy suffered from the high cost of synthesizing hundreds of thousands of probe panels. In addition, the current probe panel excluded transcripts from mitochondrial genes and ribosomal protein coding genes. This problem could be solved by expanding the probe panel.

Most SRT methods are restricted to transcripts from protein-coding genes with a main focus on polyadenylated transcripts. However, many species of non-A-tailed RNAs, such as microRNAs, newly transcribed RNAs, and long noncoding RNA and various nonhost RNAs, have many important functions. McKellar et al. developed spatial total RNA-sequencing (STRS) by integrating *in situ* polyadenylation of RNAs into the Visium protocol (Figure 9B).[45] With polyA polymerase, polyA tails could be added to all RNAs, followed by total RNA capture and analysis using conventional workflows. Such a smart design enabled the full spectrum analysis of RNAs to discern specific expression patterns of noncoding transcripts during skeletal muscle regeneration and to emphasize host transcriptional responses related to the abundance of viral RNA in localized regions. An alternative strategy for non-A-tailed transcript profiling is to spatially barcode non-polyT primers. For example, to decipher interactions of the host-microorganism and microorganism-microorganisms in spatial context, spatial host-microbiome sequencing (SHM-seq)[46] and spatial metatranscriptomics (SmT)[47] were developed by conjugating several types of capture oligos on barcoded arrays to simultaneously capture rRNAs of microbes and host mRNAs. In addition, the permeabilization protocol was optimized for better release of the bacterial RNAs. SHM-seq included an enzymatic extension reaction to transform 50% polyT capture oligos into bacterial 16S rRNA primers (Figure 9C), thereby achieving joint spatial profiling of bacterial composition and host gene expression in tissues.[46] Through application to mouse gut, SHM-seq identified gut cell subpopulations that expressed specific gene programs in different microenvironments characteristic of regional commensal bacteria, thus impacting host-bacteria interactions. For microbiome-wide spatial characterization, SmT expanded capture probes to 45% 16S rRNA capture oligos, 45% 18S rRNA/internal transcribed spacer (ITS) capture oligos, and 10% polyT capture oligos for capturing bacterial rRNAs, fungal rRNAs, and host mRNAs (Figure 9D), respectively.[47] This multimodal array enabled the capture of 962 bacterial taxa and 179 fungal taxa at the genus level. Taking *Arabidopsis thaliana* leaves as models, SmT resolved tissue-scale bacterial and fungal hotspots and the host response to these hotspots.

3.1.2. Microfluidics-Based Barcoding.
Microfluidics offers an alternative to construct spatial barcoded array, as pioneered by deterministic barcoding in tissue for spatial omics sequencing (DBiT-seq) from Fan's group (Figure 10A).[48] In DBiT-seq, a pair of microchannel chips perpendicular to each other was used to deliver polyT-tagged DNA barcodes Ai and another set of barcodes Bj into fixed tissue sections for initiating RT and ligation reactions *in situ*. At the intersections, distinct combinatorial barcodes were generated on cDNA to form a two-dimensional tissue pixel mosaic for position indexing (Figure 10A-i). The size of pixels dictated spatial resolution, and high flexibility of altering microchannel width offered resolution of 50, 25, and 10 μm to DBiT-seq. Compared with barcoded substrate-based SBS methods that

require mRNA release and diffusion into the oligo-conjugated substrate for capture, DBiT-Seq delivered barcoded oligos into permeabilized tissues to directly capture intercellular mRNAs (Figure 10A-ii). There are two factors facilitating higher detection sensitivity of DBiT-seq. First, barcoded oligos are much shorter than mRNAs with higher efficiency of tissue diffusion. Second, concentrations of barcoded oligos can be conveniently improved because they are no longer limited to the density of conjugated DNAs on substrates. Thus, DBiT-seq achieved 15.5% sensitivity, as determined by single-molecule fluorescence ISH. DBiT-seq successfully deciphered the spatial patterning of major tissue types in mouse embryos and revealed retinal pigmented epithelium and microvascular endothelium at cellular level.

This microfluidics-based combinatorial barcoding strategy also significantly reduces the variety of deterministic DNA barcodes, thereby reducing spatial barcoding costs. This strategy has been subsequently adopted for other spatial omics and spatial multiomics by transforming these omic molecules into DNA sequences and spatially barcoding them.[49−54] DNA-barcoded antibodies can label and barcode target proteins with specific DNA tags for protein sequencing.[41,48,54−57] Tn5 transposition chemistry and CUT&Tag (Cleavage Under Targets and Tagmentation) chemistry can be utilized to tag DNAs, chromatin accessibility, and histone modification for genome and epigenome sequencing, respectively.[49,52,54,58−61] For example, both DBiT-Seq[48] and spatial CITE-seq[53] enabled simultaneous spatial protein and transcriptomics profiling with protein throughput of 273[53] and the resolution of near-cellular level.[48] As for joint spatial profiling of the epigenome and transcriptome, Fan's group further developed spatial assay for transposase-accessible chromatin and RNA using sequencing (spatial ATAC-RNA-seq) and spatial assay of cleavage under targets and tagmentation and RNA using sequencing (spatial CUT&Tag-RNA-seq).[49] Similarly, Peng's group developed microfluidic indexing-based spatial assay for transposase-accessible chromatin and RNA sequencing (MISAR-seq), which allowed investigation of spatiotemporal regulatory logics during mouse brain development.[52]

To achieve multiplexed analysis of tissue samples, Wirth et al. developed the Multiplexed Deterministic Barcoding in Tissue (xDBiT) workflow (Figure 10B).[44] Serpentine microchannel chips were designed to spatially barcode nine tissue sections in parallel (Figure 10B-i). When samples in different sections are indexed using RT barcodes or indexed library preparation, tissue multiplexing can be achieved. This strategy increased the barcoded area by 4.66-fold (1.17 cm^2) compared with DBiT-seq. In addition, in light of limited reverse transcriptase and leakage risk between channels when RT reaction occurred in microchannels at 42 °C for 1.5 h in DBiT-seq, xDBiT performed RT in a whole tissue section (Figure 10B-ii) followed by two rounds of ligation reaction to introduce spatial barcode X and Y in microchannels, which required lower temperature and shorter reaction time.[62] Meanwhile, concentrations of ligase were improved by 1.5-fold. With these chemistry optimizations, xDBiT achieved a 3.0-fold increase in both read and gene counts per spot compared with DBiT-seq. xDBiT holds great potential for cost-efficient research projects on profiling 3D tissue or organ atlas and spatiotemporal expression dynamics in longitudinal studies.
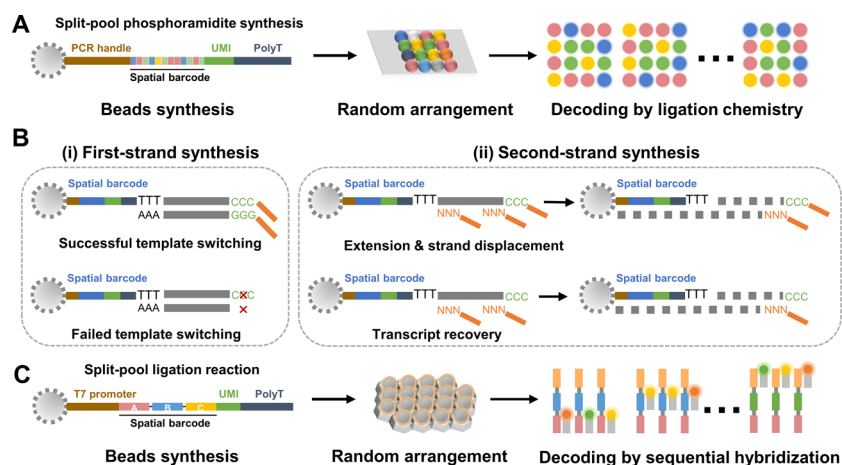
Figure 11. DNA-barcoded beads for random spatial barcoding. (A) Schematic diagram of the synthesis, random arrangement, and ligation chemistry-based decoding of barcoded beads in the Slide-seq series. (B) Second-strand synthesis using random polyN primers to recover transcripts that have failed template-switching reaction. (C) Schematic diagram of the synthesis, random arrangement, and sequential hybridization-based decoding of barcoded beads in HDST.
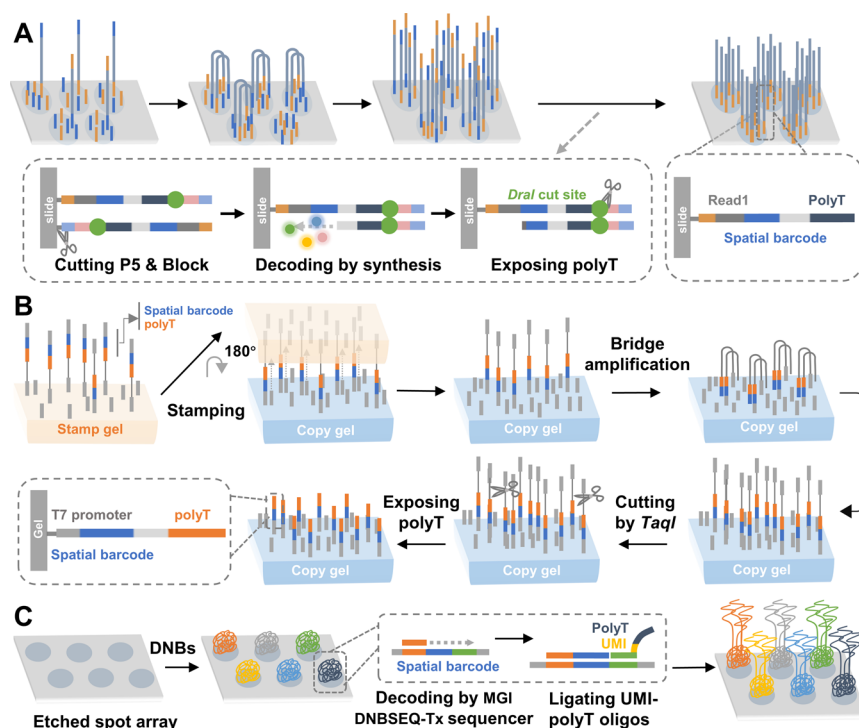

Figure 12. DNA clusters for random spatial barcoding. (A) Schematic diagram of random DNA cluster generation in illumina sequencing cell in Seq-Scope. (B) Schematic diagram of random barcoding using polony gel stamping in Pixel-seq. (C) Schematic diagram of preparation of DNA nanoball clusters using rolling circle amplification in Stereo-seq.

In situ spatial barcoding of tissues has the risk of clogging or DNA barcode leakage. Moreover, mRNAs are precross-linked to nucleic acids and proteins, which may decrease efficiency of RT reaction. To bypass this, Yang's group developed dendrimeric DNA coordinate barcoding design for spatial RNA sequencing (Decoder-seq), which adopted microfluidics-based combinatorial barcoding strategy to preassemble barcoded DNA arrays on 3D dendrimer substrates (Figure 10C-i).[63] Dendrimers have abundant active primary amino groups that enable the conjugation of a high density of amino-terminated oligos on substrate using the disuccinimidyl suberate cross-linker (Figure 10C-i). The dendrimeric substrates improved oligo densities by ∼10-fold compared

with ST and other reported SRT methods, thus facilitating a more efficient capture of mRNAs (Figure 10C-ii). Compared with *in situ* sequencing, the overall detection sensitivity of Decoder-seq was calculated to be ∼20.68%. Through application to MOBs, Decoder-seq detected ∼39% more genes than 10x Visium of similar spatial resolution. In addition, by altering the numbers and widths of microchannels, Decoder-seq offered barcoded array substrates with resolution of 50, 25, 15, and 10 μm and barcoded tissue area up to 25 mm^2. For the 15 μm spot, Decoder-seq could detect an average of 40.1 UMIs and 14.7 genes per μm^2, which is significantly higher than other cutting-edge SBS methods. Of ∼1000 total lowly expressed olfactory receptor (*Olfr*) genes, 731 could be

detected with Decoder-seq versus only 77 and ~132 using ST and 10x Visium, respectively. More importantly, the high sensitivity of Decoder-seq contributed to uncover a unique layer enrichment pattern for two *Olfr* genes, which were missed by other SBS methods.

3.2. Random Barcoding Strategies

Deterministic barcoding strategies rely on microdevices for precise delivery of spatial barcodes to specific locations, which limits the spatial resolution to the multicellular or near-cellular level. To achieve subcellular resolution, random barcoding strategies have been developed by randomly generating micro/nanoscale DNA beads or clusters on substrates to encode the corresponding positions.[50,64−69] Because of random sequences, *in situ* sequencing of DNA beads or clusters is required for position indexing.

3.2.1. DNA-Barcoded Beads.
DNA-barcoded beads are widely used to capture mRNAs of individual cells for cell barcoding during scRNA-seq. Similarly, DNA-barcoded beads can be packed on substrates in a monolayer manner to encode positions, and spatial resolution can be improved by reducing the bead sizes. For example, Chen's group developed Slide-seq series for SRT and spatial multiomics by densely packing 10 μm DNA-barcoded beads onto a rubber-coated glass coverslip (Figure 7B and Figure 11A).[50,65,70] In Slide-seq, the DNA beads were fabricated by split-pool phosphoramidite synthesis and decoded through sequencing by ligation chemistry,[65] whereby 65.8 ± 1.4% of beads was calculated to match with a single cell type.[62] In consideration of inefficiency of the template-switching reaction that adds a 3′-priming site for whole-transcriptome amplification,[59] Chen's group developed Slide-seqV2 by adding a second-strand synthesis step with random polyN primers into library preparation (Figure 11B).[66] Slide-seqV2 achieved ~50% RNA capture efficiency compared with that of scRNA-seq, ~10-fold greater than that of Slide-seq.

To produce subcellular resolution, Lundeberg's group developed high-definition spatial transcriptomics (HDST) by using 2 μm DNA-barcoded beads for spatial barcoding (Figure 7B and Figure 11C).[71] The beads were fabricated by a split-and-pool ligation reaction and decoded via sequential hybridization. Because of subcellular features, HDST was successfully applied to identify transcripts with preferential nuclear localization. Nevertheless, with this type of barcoded method, it was challenging to reach submicrometer spatial resolution because of the technical difficulty of synthesizing and densely packing nanoscale DNA beads.

3.2.2. DNA Clusters.
Efficient amplification reaction of DNAs has been leveraged to produce submicrometer DNA clusters for spatial barcoding. Solid-phase bridge amplification can generate numerous tightly packed DNA clusters from individual oligos on PCR adapter-modified substrates and has been utilized in illumina sequencing technology. Inspired by this, Cho et al. developed Seq-Scope by utilizing a flow cell of illumina sequencing platform to randomly produce DNA clusters (Figure 12A).[68] The oligonucleotide "seed" molecules contained PCR/read adaptor, unique spatial barcode, and the *DraI* restriction enzyme-cleavable polyT oligos. The spatial barcodes of DNA clusters could be read out during the sequencing-by-synthesis procedure for position indexing. After *DraI* digestion, polyT was exposed for subsequent mRNA capture and SRT analysis following the traditional protocol. Because of localized amplification of bridge amplification, Seq-

Scope achieved up to 1.5 million clusters per mm² with center-to-center resolution of ~0.6 μm on average (Figure 7B). Using image segmentation to identify single-cell areas from a hematoxylin and eosin (H&E) image, the transcriptome output of Seq-Scope was calculated to be ~4700 UMIs per cell on average, which is comparable with conventional scRNA-seq.Seq-Scope visualized spatial transcriptome heterogeneity at multiple histological scales, including tissue zonation, cellular components, and subcellular architectures.

The process of decoding spatial barcode sequences is costly and time-consuming, which poses challenges for upscaling the array production. To solve this problem, Gu's group developed polony-indexed library-sequencing (Pixel-seq), which enabled repeatable and scalable replication of DNA cluster arrays (i.e., polonies) using polony gel stamping (Figure 7B and Figure 12B).[69] Polonies were fabricated by the abovementioned bridge amplification on an elastomeric and cross-linked polyacrylamide gel, just like a stamp. Polonies acted as templates and could be copied to many "copy gels" by DNA polymerase-catalyzed chain extension. The gel-to-gel replication reliably maintained original resolution and sequence information due to covalent conjugation of primers and templates without DNA diffusion. Moreover, decoding sequencing was required for only one or a few gels for a series of copies. In addition, because of the decreased gel constraints on the bridge amplification, high-density polonies (~0.6−0.8 million per mm²) could be formed in a continuous distribution manner with feature diameter of ~1 μm and minimal feature-to-feature gaps (Figure 7B). After cell segmentation, Pixel-seq enabled detection of 3346 and 6458 UMIs for each periglomerular-type cell and each mitral/tufted cell, respectively.

Rolling circle amplification (RCA) can generate DNA nanoball (DNB) clusters with numerous repetitive sequences for spatial barcoding. On the basis of the DNB sequencing technique, Chen et al. developed spatially enhanced-resolution omics-sequencing (Stereo-seq) with the advantages of high-spatial resolution, high sensitivity, and large-area barcoded array (Figure 12C).[67] DNBs were electrostatically adsorbed onto the photolithographically etched spot array with a spot diameter of ~220 nm and center-to-center distances of 500 to 715 nm (Figure 7B). Using the MGI DNBSEQ-Tx sequencer, the random barcodes of DNBs could be sequenced to determine spatial barcodes (i.e., coordinate identity). Then, UMI-polyT oligomers were ligated to DNBs for subsequent SRT study. When binning spots to 10 μm equivalent to medium cell size, Stereo-seq captured 1450 UMIs. More importantly, this sequencer allowed sequencing of large area chips, which enabled the generation of a large-area barcoded array (13.2 cm × 13.2 cm). Thus, Stereo-seq successfully mapped a transcriptomic atlas of mouse organogenesis. Although these random barcoding methods achieved submicrometer resolution, they depended on complex algorithms to cluster bins and segment cell boundaries for single-cell analysis.

3.3. Single Cell/Nucleus RNA-seq-Assisted Spatial Barcoding Strategies

The aforementioned spatial barcoding strategies leverage primer oligos from barcoded pixels to spatially barcode mRNAs. In the low-resolution mode, each pixel captures mRNA from multiple cells. In high-resolution mode, the determination of cell boundaries becomes challenging, and
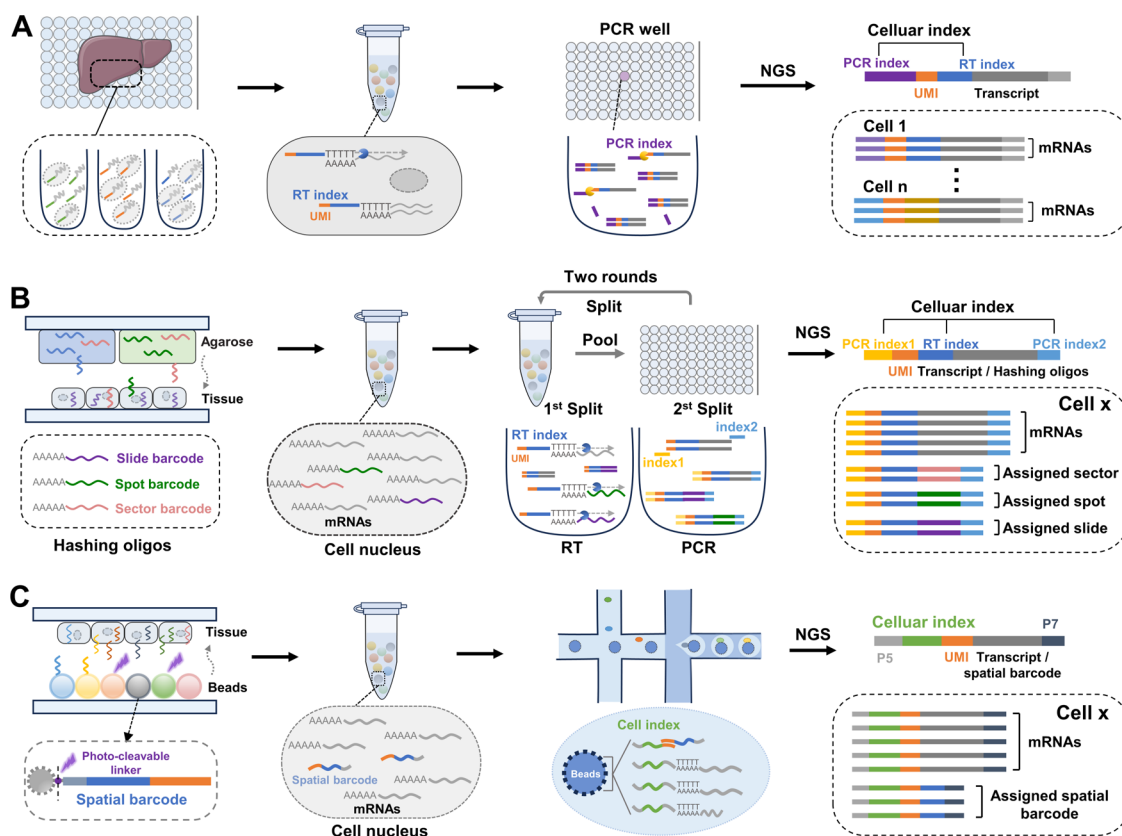
Figure 13. Spatial barcoding of individual cells assisted by scRNA-seq or snRNA-seq for single-cell spatial transcriptome analysis. (A) Workflow of spatial barcoding of individual cells in XYZeq, including two rounds of split-pool cell barcoding: RT and PCR. (B) Workflow of sci-Space in which three types of polyA-tailed hashing oligos were used to spatially barcode cell nuclei and sequenced along mRNAs at single-cell resolution via sci-RNA-seq. (C) Workflow of Slide-tags in which spatial barcodes were photocleaved from DNA-barcoded beads to label cell nuclei and further sequenced along mRNAs via droplet-based snRNA-seq.

each pixel may capture mixtures of transcriptomes from adjacent cells. Thus, none of these methods is able to truly resolve a single-cell spatial transcriptome and they all depend on computational methods to deconvolve or perform binning to identify cell types and marker genes with limited accuracy.[72] Recently, scRNA-seq or snRNA-seq-assisted spatial barcoding strategies have been developed to realize true single-cell SRT profiling (Figure 13).[38,54,55] Generally, barcode DNAs are introduced into tissue cells or nuclei from a spatially barcoded array, which are read out along cDNAs of mRNAs through high-throughput scRNA-seq after tissue dissociation.

3.3.1. Split-Pool-Based Spatial Barcoding. Split-pool barcoding strategy is widely applied in high-throughput scRNA-seq and snRNA-seq, which uses multiple rounds of DNA barcoding of pool and split samples to generate a large collection of unique combinatorial identifiers for individual cell or nuclei labeling. This strategy can be readily expanded to spatial barcoding at the single-cell level. Lee et al. developed XYZeq for spatially resolved scRNA-seq of tumor tissues (Figure 13A).[73] First, a cryo-preserved tissue section was mounted on the microwell chip to be physically partitioned into corresponding microwells of 500 μm in diameter, which contained distinct barcoded RT primers and mix, as well as digestion reagents. After RT and tissue digestion, the labeled individual cells were pooled and further split into wells for PCR using barcoded primers. Thus, with two rounds of split-pool indexing, the resultant RT index and PCR index could act together as a combinatorial cell barcode, and the RT index

acted as a spatial barcode. After sequencing, the recovered single cells could be mapped back to their original locations for SRT analysis. Through application to the mouse tumor model, XYZeq identified a migration-associated transcriptomic program in tumor-associated mesenchymal stem cells and revealed that the expression pattern of tumor suppressor genes was consistent with the spatial trajectory. However, XYZeq still required barcoded oligos to spatially barcode mRNAs, and the mRNA detection sensitivity was codetermined by the efficiencies of oligo diffusion into cells, RT using barcoded primers, and scRNA-seq. Only reads with both spatial barcodes and cell barcodes could be considered valid, which resulted in low UMI (<1600 UMIs per cell) and gene (<700 genes per cell) recovery.

Trapnell's group developed sci-Space to conduct embryo-scale, single-cell spatial transcriptomics in which spatial barcodes were transferred into nuclei only for cell hashing (Figure 13B).[74] With a microarray scanner, hashing oligos, including sector barcodes and spot barcodes, were spotted on agarose-coated slides for hierarchically combinatorial barcoding of positions. Each position was marked by a unique combination of one sector barcode and one spot barcode. The formed space grid array contained 7056 uniquely barcoded spots with a barcoded area of 18 × 18 mm^2, spot diameter of ~75 μm, and center-to-center distance of 200 μm. Tissue sections were permeabilized with polyA-tailed section barcodes and then physically juxtaposed to a glass slide bearing the spatially gridded hashing oligos. With diffusion, polyA-tailed

hashing oligos were transferred to tissue nuclei, and the disassociated nuclei were subjected to single-cell combinatorial indexing RNA sequencing (sci-RNA-seq).[75] This design allowed parallel labeling of cell barcodes on hashing oligos and cDNAs for simultaneous position indexing and mRNA measurement, which facilitated sensitive gene detection. Sector and spot barcodes were used for position indexing, and sector barcodes were used to trace different tissue sections. In sci-Space, a mean of 2514 UMIs and a mean of 1231 genes could be detected per nucleus. These were substantially higher than those detected in XYZeq. They applied sci-Space to two samples of embryonic day 14 (E14.0) mouse embryo and revealed spatially regulated gene expression and neuronal migration dynamics.

3.3.2. Droplet-Based Spatial Barcoding.
The pixel sizes of XYZeq and sci-Space are limited to tens to hundreds of microns. Although several cells in the same pixels are distinguished with scRNA-seq, the arrangement and inter-actions among these adjacent cells are still unknown. To bridge this gap, Chen's group developed Slide-tags by tagging cellular nuclei of an intact tissue section with spatial barcode oligos that were photocleaved from their classical 10 μm DNA-barcoded bead substrates (Figure 13C).[50] The dissociated nuclei were associated with spatial barcodes, which could serve as inputs for mature snRNA-seq for the simultaneous readout of omics molecules and spatial barcodes. With the algorithm, individual nuclei were assigned a spatial coordinate. Compared with XYZeq and sci-Space, spatial resolution of Slide-tags improved by a factor of 20 to 50. Moreover, Slide-tags reduced cell loss with 4.5-fold more recovered nuclei per unit area because it was free of multiple rounds of split-and-pool cell barcoding. More importantly, 1.8-fold more UMIs and 1.7-fold more genes could be detected per nucleus using Slide-tags compared with sci-Space. In Slide-tags, transcripts and spatial barcodes were completely released for the homogeneous phase reaction using droplet-based snRNA-seq, thus avoiding inefficiency of the intercellular cell barcoding reaction. Slide-tags directly resolved biomolecular information at intrinsically single-cell resolution, which avoided complex data processing, such as deconvolution and segmentation. Moreover, combined with standard 10x Genomics Multiome workflows, Slide-tags enabled spatial multiomics. Barcoded oligos just served as spatial tags and sequenced along with omics molecules so that Slide-tags avoided competitive spatial barcoding reactions among multiomic molecules for high-detection sensitivity. Through application to metastatic melanoma, Slide-tags comeasured open chromatin, mRNAs and T cell receptors, and identified transcription factor motifs, which induce cancer cell-state transitions in spatially distinct microenvironment.

This type of spatial barcoding strategies recovers true single-cell transcriptomes, which can accurately reveal patterns of spatial gene regulation of specific cell types and estimate the functions of each cell type in different anatomical regions. Moreover, their single-cell transcriptome data can be readily integrated with nonspatial scRNA-seq or snRNA-seq data for rapid and accurate annotation of diverse cell types and spatial mapping. Although powerful, there are three main challenges. First, tissue dissociation and scRNA-seq or snRNA-seq procedures induce substantial loss of cells and nuclei, thereby omitting some critical information. For example, sci-Space and Slide-tags only recovered 2.2% and 25% of total nuclei, respectively. Second, tissue fixation and permeabilization are commonly required for diffusing spatial barcodes into cells or

nuclei. The fixed mRNAs and/or corresponding cDNAs would be lost under enzyme treatment during tissue dissociation. Third, their detection sensitivities are commonly lower than those of scRNA-seq or snRNA-seq, probably because of RNA degradation from the long-term tissue preservation and spatial barcoding procedure, as well as competitive reaction between mRNAs and barcoded oligos during cell barcoding. More efforts should be devoted to improving the cell recovery rate and detection sensitivity.

4. CONCLUSION AND OUTLOOK

Multicellular organisms consist of diverse cells arranged in intricate 3D structures where the cell composition, distribution, and intercellular interactions significantly influence tissue function. However, the cell-type composition and organization remain largely unknown for most organisms. In the past two decades, extensive endeavors have been dedicated to unraveling the intricacies of the tissue atlas. In particular, advancements in sequencing chemistry and barcoding chemistry have yielded a wealth of comprehensive and multidimensional molecular information. NGS stands as a powerful tool for high-throughput sequencing and processes thousands and millions of sequences per run. High-throughput scRNA-seq is further developed using cell barcoding strategies to identify cell types and states. With spatial indexing and barcoding techniques, SRT methods are emerging to profile gene expression in the tissue spatial context, thereby empowering a new generation of scientific discoveries. This Perspective has focused on NGS-based SRT techniques, including ORS and SBS, which enable high-throughput and genome-wide profiling of mRNAs compared with imaging-based SRT techniques.

Spatial indexing and barcoding are the key premise for SRT techniques, and barcoding reaction affects barcoding through-put, detection sensitivity, and spatial resolution. First, SBS methods exhibit overwhelming advantages in the throughput of spatial barcoding reaction over ORS methods. To achieve multiplex position barcoding for ORS methods, spatially resolved iterative illumination is required to sequentially initiate photochemical reactions for corresponding ROI labeling, which is time-consuming, tedious, and low-through-put. In contrast, SBS leverages a spatially barcoded array to simultaneously label almost all positions of the tissue section with DNA barcodes. Spatial coordinates are converted to sequence barcodes, which are read out by NGS in a high-throughput manner. Second, the detection sensitivity of SBS methods is more affected by barcoding reaction efficiency than are ORS methods. Most ORS methods leverage photosensitive tags to label cells, except those based on spatial labeling of mRNAs in ROIs.[33,35,36,77] Reaction efficiency of tag labeling affects only cell recovery but does not affect mRNA detection sensitivity. In contrast, most of the SBS methods rely on barcoded oligos to spatially barcode mRNAs, and the efficiency of the barcoding reaction directly determines the percentage of mRNAs to be recovered and detected. As a result, detection sensitivity of SBS is inferior to that of ORS. Third, the spatial resolution of the barcoding reaction in both ORS and SBS methods is theoretically the diffraction limit but is far from being realized at present. In ORS methods, the size of light spots determines spatial resolution of the barcoding reaction, but light-scattering induces an out-of-ROI reaction. In SBS methods, the finer barcoded array relies on imaging-based decoding of spatial barcodes. Their final spatial resolutions are

affected by diffusion distance of mRNAs, commonly at micrometer scale.[67] With different spatial barcoding strategies, ORS and SBS methods have their own strengths and weaknesses, and researchers can choose the appropriate method according to the application requirements. In addition, the ORS and SBS methods can complement each other. For example, whole tissue sections can undergo high-throughput analysis by using SBS to identify some important ROIs. Cells in these ROIs, even rare cell types, can then undergo further in-depth analysis with ORS methods at single-cell or subcellular resolution.

In light of the important role of the spatial barcoding reaction in SRT performance, many endeavors have been made to improve multiplex capacity and efficiency of the barcoding reaction in the past few years. Color barcodes and DNA barcodes have been adopted in ZipSeq[29] and Light-Seq[36] in which multiple rounds of photouncaging or photo-cross-linking reactions allow improvement of multiplex capacity of spatial barcoding for ORS methods. To improve sensitivity, SBS methods have employed two types of strategies. The first is the use of spatial barcoded oligos for cell labeling followed by scRNA-seq or snRNA-seq[50,74] Spatial barcodes and mRNAs are sequenced in parallel to facilitate high-sensitive mRNA detection.[50] The second strategy is improvement of efficiencies of multiple-step reactions during spatial barcoding of mRNAs, including mRNA capture,[40,44,45,48,63] RT,[41,62] and second-strand synthesis.[66,68] With these improvements, existing NGS-based SRT methods achieve high-sensitivity (approaching that of scRNA-seq methods), high-resolution (submicrometer level), and high-throughput (centimeter-scaled barcoded area) transcriptomic profiling, which has revolutionized the fields of developmental biology, neuroscience, oncology, and histopathology.

Despite ongoing advances, SRT techniques are still at the dawn of the spatial omics era. The ultimate goal of spatial omics is to measure the abundance of all genes and gene isoforms, as well as multimodel omics molecules at subcellular resolution and spatiotemporal multidimension in 3D tissues. First, in order to achieve sensitive total transcriptome analysis, spatially barcoded cells can be combined with newly emerging single-nucleus/cell total RNA sequencing techniques.[78−80] Alternatively, new spatial barcoding strategies should be developed to barcode the full spectrum of RNAs, such as expanding the probe pane and adopting random primers. It should be mentioned that the amount of total RNAs is much larger than that of polyA-tailed mRNAs. Thus, many more barcoded oligos should be conjugated or delivered in the spatially barcoded array, and the efficiency of the barcoding reaction should be further improved. In addition, spatially barcoded sequences could be read out via long-read third-generation sequencing to reveal structural variants of RNAs and to identify the specificity and diversity of B and T cell antigen receptors.[81,82]

Second, to improve the accuracy and resolution of spatial barcoding in ORS methods, photomasks slightly smaller than the intended ROIs could be designed to mitigate light-scattering effects. Laser-based point-scanning microscopes could be used to replace DMD for higher barcoding resolution, but illumination is much slower. As for SBS methods, micro/nanofabrication technologies can be adopted to generate a barcoded array of higher resolution. Engineering the barcoded array with favorable hybridization kinetics enables rapid capture of mRNAs to reduce mRNA diffusion distance for more accurate spatial barcoding. In addition, the new expansion microscopy technique enables ∼10-fold expansion of tissues and, thus, facilitates imaging with ∼25 nm resolution using a traditional optical microscope.[83] Combined with this technique, the resolution of both ORS and SBS methods could be up to the nanometer scale.

Third, as for multimodal spatial omics, some cutting-edge dual-omics methodologies have been developed.[48−54] However, triple-omics and other multimodal spatial omics methodologies have rarely been reported. The main challenge is how to efficiently capture and accurately barcode these extremely large amounts of omics molecules in spatial context; more efforts should be devoted in this direction. In addition, gene expression is a dynamic process. Combined with metabolic RNA labeling techniques, newly transcribed RNAs can be labeled and distinguished from pre-existing RNAs during SRT analysis to provide spatiotemporal multidimensional molecular information.[84]

Fourth, a 3D spatial omics methodology is needed to profile whole organs or even organisms. Most existing SRT methods are applicable only to thin tissue sections. For 3D profiling, serial sections are analyzed for reconstruction of a 3D cube using computational methods. This is time-consuming and expensive and not true 3D profiling. In the future, 3D spatial barcoding techniques should be developed. For example, serial two-photon or near-infrared tomography and light sheet microscopy may allow 3D spatial barcoding with the elaborate design of photosensitive probes. Finally, the SRT methods are expected to be more accessible to customers by reducing cost, simplifying the procedure, and improving reliability and robustness. In addition, commercial adoption will increase access and use of SRT technologies. Overall, with all these revolutions and advancements, SRT technologies will provide powerful and exciting tools to reveal comprehensive and multidimensional molecular landscapes for studies of complex biological processes.

■ AUTHOR INFORMATION

Corresponding Authors

Lingling Wu − *Institute of Molecular Medicine, Shanghai Key Laboratory for Nucleic Acid Chemistry and Nanomedicine, Renji Hospital, Shanghai Jiao Tong University School of Medicine, Shanghai 200127, China;* ⊙ orcid.org/0000-0001-8738-0357; Email: llwu@shsmu.edu.cn

Chaoyong Yang − *Institute of Molecular Medicine, Shanghai Key Laboratory for Nucleic Acid Chemistry and Nanomedicine, Renji Hospital, Shanghai Jiao Tong University School of Medicine, Shanghai 200127, China; The MOE Key Laboratory of Spectrochemical Analysis & Instrumentation, Discipline of Intelligent Instrument and Equipment, Department of Chemical Biology, College of Chemistry and Chemical Engineering, Xiamen University, Xiamen 361005, China; State Key Laboratory of Cellular Stress Biology, School of Life Sciences, Faculty of Medicine and Life Sciences, Xiamen University, Xiamen 361102, China;* ⊙ orcid.org/0000-0002-2374-5342; Email: cyyang@xmu.edu.cn

Authors

Weixiong Shi − *Institute of Molecular Medicine, Shanghai Key Laboratory for Nucleic Acid Chemistry and Nanomedicine, Renji Hospital, Shanghai Jiao Tong University School of Medicine, Shanghai 200127, China; The MOE Key*

Laboratory of Spectrochemical Analysis & Instrumentation, Discipline of Intelligent Instrument and Equipment, Department of Chemical Biology, College of Chemistry and Chemical Engineering, Xiamen University, Xiamen 361005, China

Jing Zhang − *State Key Laboratory of Cellular Stress Biology, School of Life Sciences, Faculty of Medicine and Life Sciences, Xiamen University, Xiamen 361102, China*

Shanqing Huang − *The MOE Key Laboratory of Spectrochemical Analysis & Instrumentation, Discipline of Intelligent Instrument and Equipment, Department of Chemical Biology, College of Chemistry and Chemical Engineering, Xiamen University, Xiamen 361005, China*

Qian Fan − *Institute of Molecular Medicine, Shanghai Key Laboratory for Nucleic Acid Chemistry and Nanomedicine, Renji Hospital, Shanghai Jiao Tong University School of Medicine, Shanghai 200127, China*

Jiao Cao − *Institute of Molecular Medicine, Shanghai Key Laboratory for Nucleic Acid Chemistry and Nanomedicine, Renji Hospital, Shanghai Jiao Tong University School of Medicine, Shanghai 200127, China*

Jun Zeng − *Institute of Molecular Medicine, Shanghai Key Laboratory for Nucleic Acid Chemistry and Nanomedicine, Renji Hospital, Shanghai Jiao Tong University School of Medicine, Shanghai 200127, China*

Complete contact information is available at:
https://pubs.acs.org/10.1021/jacsau.4c00118

Author Contributions

Notes

The authors declare no competing financial interest.

■ ACKNOWLEDGMENTS

■ REFERENCES

(1) Slack, J. M. W. Origin of Stem Cells in Organogenesis. *Science* **2008**, *322* (5907), 1498−1501.

(2) Fridman, W. H.; Zitvogel, L.; Sautès−Fridman, C.; Kroemer, G. The Immune Contexture in Cancer Prognosis and Treatment. *Nat. Rev. Clin. Oncol.* **2017**, *14* (12), 717−734.

(3) Ozsolak, F.; Milos, P. M. RNA Sequencing: Advances, Challenges and Opportunities. *Nat. Rev. Genet.* **2011**, *12* (2), 87−98.

(4) Wu, A. R.; Wang, J.; Streets, A. M.; Huang, Y. Single-Cell Transcriptional Analysis. *Annu. Rev. Anal. Chem.* **2017**, *10*, 439−462.

(5) Wang, Y.; Navin, N. E. Advances and Applications of Single-Cell Sequencing Technologies. *Mol. Cell* **2015**, *58* (4), 598−609.

(6) Zeng, H.; Huang, J.; Ren, J.; Wang, C. K.; Tang, Z.; Zhou, H.; Zhou, Y.; Shi, H.; Aditham, A.; Sui, X.; Chen, H.; Lo, J. A.; Wang, X.

(7) Lubeck, E.; Coskun, A. F.; Zhiyentayev, T.; Ahmad, M.; Cai, L. Single-Cell in Situ RNA Profiling by Sequential Hybridization. *Nat. Methods* **2014**, *11* (4), 360−361.

(8) Eng, C.-H. L.; Lawson, M.; Zhu, Q.; Dries, R.; Koulena, N.; Takei, Y.; Yun, J.; Cronin, C.; Karp, C.; Yuan, G.-C.; et al. Transcriptome-Scale Super-Resolved Imaging in Tissues by RNA seqFISH+. *Nature* **2019**, *568* (7751), 235−239.

(9) Ke, R.; Mignardi, M.; Pacureanu, A.; Svedlund, J.; Botling, J.; Wählby, C.; Nilsson, M. In Situ Sequencing for RNA Analysis in Preserved Tissue and Cells. *Nat. Methods* **2013**, *10* (9), 857−860.

(10) Larsson, L.; Frisén, J.; Lundeberg, J. Spatially Resolved Transcriptomics Adds a New Dimension to Genomics. *Nat. Methods* **2021**, *18* (1), 15−18.

(11) Moses, L.; Pachter, L. Museum of Spatial Transcriptomics. *Nat. Methods* **2022**, *19* (5), 534−546.

(12) Rao, A.; Barkley, D.; França, G. S.; Yanai, I. Exploring Tissue Architecture Using Spatial Transcriptomics. *Nature* **2021**, *596* (7871), 211−220.

(13) Bonner, R. F.; Emmert-Buck, M.; Cole, K.; Pohida, T.; Chuaqui, R.; Goldstein, S.; Liotta, L. A. Laser Capture Micro-dissection: Molecular Analysis of Tissue. *Sci. New Ser.* **1997**, *278* (5342), 1481−1483.

(14) Emmert-Buck, M. R.; Bonner, R. F.; Smith, P. D.; Chuaqui, R. F.; Zhuang, Z.; Goldstein, S. R.; Weiss, R. A.; Liotta, L. A. Laser Capture Microdissection. *Science* **1996**, *274*, 998−1001.

(15) Schutze, K.; Lahr, G. Identification of Expressed Genes by Laser-mediated manipulation of Single Cells. *Nat. Biotechnol.* **1998**, *16*, 737−742.

(16) Chung, C. Y.; Seo, H.; Sonntag, K. C.; Brooks, A.; Lin, L.; Isacson, O. Cell Type-Specific Gene Expression of Midbrain Dopaminergic Neurons Reveals Molecules Involved in Their Vulnerability and Protection. *Hum. Mol. Genet.* **2005**, *14* (13), 1709−1725.

(17) Kadkhodaei, B.; Alvarsson, A.; Schintu, N.; Ramsköld, D.; Volakakis, N.; Joodmardi, E.; Yoshitake, T.; Kehr, J.; Decressac, M.; Björklund, A.; Sandberg, R.; Svenningsson, P.; Perlmann, T. Transcription Factor Nurr1Maintains Fiber Integrity and Nuclear-Encoded Mitochondrial Gene Expression in Dopamine Neurons. *Proc. Natl. Acad. Sci. U. S. A.* **2013**, *110* (6), 2360−2365.

(18) Picelli, S.; Björklund, Å. K.; Faridani, O. R.; Sagasser, S.; Winberg, G.; Sandberg, R. Smart-Seq2 for Sensitive Full-Length Transcriptome Profiling in Single Cells. *Nat. Methods* **2013**, *10* (11), 1096−1098.

(19) Nichterwitz, S.; Chen, G.; Aguila Benitez, J.; Yilmaz, M.; Storvall, H.; Cao, M.; Sandberg, R.; Deng, Q.; Hedlund, E. Laser Capture Microscopy Coupled with Smart-Seq2 for Precise Spatial Transcriptomic Profiling. *Nat. Commun.* **2016**, *7* (1), 12139.

(20) Moor, A. E.; Harnik, Y.; Ben-Moshe, S.; Massasa, E. E.; Rozenberg, M.; Eilam, R.; Halpern, K. B.; Itzkovitz, S. Spatial Reconstruction of Single Enterocytes Uncovers Broad Zonation along the Intestinal Villus Axis. *Cell* **2018**, *175* (4), 1156−1167.

(21) Baccin, C.; Al-Sabah, J.; Velten, L.; Helbling, P. M.; Grünschläger, F.; Hernández-Malmierca, P.; Nombela-Arrieta, C.; Steinmetz, L. M.; Trumpp, A.; Haas, S. Combined Single-Cell and Spatial Transcriptomics Reveal the Molecular, Cellular and Spatial Bone Marrow Niche Organization. *Nat. Cell Biol.* **2020**, *22* (1), 38−48.

(22) Chen, J.; Suo, S.; Tam, P. P.; Han, J.-D. J.; Peng, G.; Jing, N. Spatial Transcriptomic Analysis of Cryosectioned Tissue Samples with Geo-Seq. *Nat. Protoc.* **2017**, *12* (3), 566−580.

(23) Peng, G.; Suo, S.; Chen, J.; Chen, W.; Liu, C.; Yu, F.; Wang, R.; Chen, S.; Sun, N.; Cui, G.; et al. Spatial Transcriptome for the Molecular Annotation of Lineage Fates and Cell Identity in Mid-Gastrula Mouse Embryo. *Dev. Cell* **2016**, *36* (6), 681−697.

(24) Peng, G.; Suo, S.; Cui, G.; Yu, F.; Wang, R.; Chen, J.; Chen, S.; Liu, Z.; Chen, G.; Qian, Y.; et al. Molecular Architecture of Lineage

Allocation and Tissue Organization in Early Mouse Embryo. *Nature* **2019**, *572* (7770), 528−532.

(25) Medaglia, C.; Giladi, A.; Stoler-Barak, L.; De Giovanni, M.; Salame, T. M.; Biram, A.; David, E.; Li, H.; Iannacone, M.; Shulman, Z.; et al. Spatial Reconstruction of Immune Niches by Combining Photoactivatable Reporters and scRNA-Seq. *Science* **2017**, *358* (6370), 1622−1626.

(26) Jaitin, D. A.; Kenigsberg, E.; Keren-Shaul, H.; Elefant, N.; Paul, F.; Zaretsky, I.; Mildner, A.; Cohen, N.; Jung, S.; Tanay, A.; Amit, I. Massively Parallel Single-Cell RNA-Seq for Marker-Free Decomposition of Tissues into Cell Types. *Science* **2014**, *343* (6172), 776−779.

(27) Genshaft, A. S.; Ziegler, C. G. K.; Tzouanas, C. N.; Mead, B. E.; Jaeger, A. M.; Navia, A. W.; King, R. P.; Mana, M. D.; Huang, S.; Mitsialis, V.; Snapper, S. B.; Yilmaz, Ö. H.; Jacks, T.; Van Humbeck, J. F.; Shalek, A. K. Live Cell Tagging Tracking and Isolation for Spatial Transcriptomics Using Photoactivatable Cell Dyes. *Nat. Commun.* **2021**, *12* (1), 4995.

(28) Tang, Q.; Liu, L.; Guo, Y.; Zhang, X.; Zhang, S.; Jia, Y.; Du, Y.; Cheng, B.; Yang, L.; Huang, Y.; Chen, X. Optical Cell Tagging for Spatially Resolved Single-Cell RNA Sequencing. *Angew. Chem., Int. Ed.* **2022**, *61* (7), No. e202113929.

(29) Hu, K. H.; Eichorst, J. P.; McGinnis, C. S.; Patterson, D. M.; Chow, E. D.; Kersten, K.; Jameson, S. C.; Gartner, Z. J.; Rao, A. A.; Krummel, M. F. ZipSeq: Barcoding for Real-Time Mapping of Single Cell Transcriptomes. *Nat. Methods* **2020**, *17* (8), 833−843.

(30) van der Leun, A. M.; Hoekstra, M. E.; Reinalda, L.; Scheele, C. L.; Toebes, M.; van de Graaff, M. J.; Chen, L. Y.; Li, H.; Bercovich, A.; Lubling, Y.; et al. Single-Cell Analysis of Regions of Interest (SCARI) Using a Photosensitive Tag. *Nat. Chem. Biol.* **2021**, *17* (11), 1139−1147.

(31) Bues, J.; Biočanin, M.; Pezoldt, J.; Dainese, R.; Chrisnandy, A.; Rezakhani, S.; Saelens, W.; Gardeux, V.; Gupta, R.; Sarkis, R.; et al. Deterministic scRNA-Seq Captures Variation in Intestinal Crypt and Organoid Composition. *Nat. Methods* **2022**, *19* (3), 323−330.

(32) Lovatt, D.; Ruble, B. K.; Lee, J.; Dueck, H.; Kim, T. K.; Fisher, S.; Francis, C.; Spaethling, J. M.; Wolf, J. A.; Grady, M. S.; Ulyanova, A. V.; Yeldell, S. B.; Griepenburg, J. C.; Buckley, P. T.; Kim, J.; Sul, J.-Y.; Dmochowski, I. J.; Eberwine, J. Transcriptome in Vivo Analysis (TIVA) of Spatially Defined Single Cells in Live Tissue. *Nat. Methods* **2014**, *11* (2), 190−196.

(33) Honda, M.; Oki, S.; Kimura, R.; Harada, A.; Maehara, K.; Tanaka, K.; Meno, C.; Ohkawa, Y. High-Depth Spatial Transcriptome Analysis by Photo-Isolation Chemistry. *Nat. Commun.* **2021**, *12* (1), 4416.

(34) Hashimshony, T.; Senderovich, N.; Avital, G.; Klochendler, A.; De Leeuw, Y.; Anavy, L.; Gennert, D.; Li, S.; Livak, K. J.; Rozenblatt-Rosen, O.; et al. CEL-Seq2: Sensitive Highly-Multiplexed Single-Cell RNA-Seq. *Genome Biol.* **2016**, *17* (1), 77.

(35) Merritt, C. R.; Ong, G. T.; Church, S. E.; Barker, K.; Danaher, P.; Geiss, G.; Hoang, M.; Jung, J.; Liang, Y.; McKay-Fleisch, J.; et al. Multiplex Digital Spatial Profiling of Proteins and RNA in Fixed Tissue. *Nat. Biotechnol.* **2020**, *38* (5), 586−599.

(36) Kishi, J. Y.; Liu, N.; West, E. R.; Sheng, K.; Jordanides, J. J.; Serrata, M.; Cepko, C. L.; Saka, S. K.; Yin, P. Light-Seq: Light-Directed in Situ Barcoding of Biomolecules in Fixed Cells and Tissues for Spatially Indexed Sequencing. *Nat. Methods* **2022**, *19* (11), 1393−1402.

(37) Yurke, B.; Turberfield, A. J.; Mills, A. P., Jr; Simmel, F. C.; Neumann, J. L. A DNA-Fuelled Molecular Machine Made of DNA. *Nature* **2000**, *406* (6796), 605−608.

(38) Nakamura, S.; Kawabata, H.; Fujimoto, K. Double Duplex Invasion of DNA Induced by Ultrafast Photo-Cross-Linking Using 3-Cyanovinylcarbazole for Antigene Methods. *Chem. Commun.* **2017**, *53* (54), 7616−7619.

(39) Ståhl, P. L.; Salmén, F.; Vickovic, S.; Lundmark, A.; Navarro, J. F.; Magnusson, J.; Giacomello, S.; Asp, M.; Westholm, J. O.; Huss, M.; et al. Visualization and Analysis of Gene Expression in Tissue

Sections by Spatial Transcriptomics. *Science* **2016**, *353* (6294), 78−82.

(40) Fan, Y.; Andrusivová, Ž.; Wu, Y.; Chai, C.; Larsson, L.; He, M.; Luo, L.; Lundeberg, J.; Wang, B. Expansion Spatial Transcriptomics. *Nat. Methods* **2023**, *20* (8), 1179−1182.

(41) Vickovic, S.; Lötstedt, B.; Klughammer, J.; Mages, S.; Segerstolpe, Å.; Rozenblatt-Rosen, O.; Regev, A. SM-Omics Is an Automated Platform for High-Throughput Spatial Multi-Omics. *Nat. Commun.* **2022**, *13* (1), 795.

(42) Ben-Chetrit, N.; Niu, X.; Swett, A. D.; Sotelo, J.; Jiao, M. S.; Stewart, C. M.; Potenski, C.; Mielinis, P.; Roelli, P.; Stoeckius, M.; Landau, D. A. Integration of Whole Transcriptome Spatial Profiling with Protein Markers. *Nat. Biotechnol.* **2023**, *41* (6), 788−793.

(43) 10x Genomics. *Spatial Gene Expression for FFPE - Official 10x Genomics Support.* https://www.10xgenomics.com/cn/support/spatial-gene-expression-ffpe (accessed 2024-02-02).

(44) Mirzazadeh, R.; Andrusivova, Z.; Larsson, L.; Newton, P. T.; Galicia, L. A.; Abalo, X. M.; Avijgan, M.; Kvastad, L.; Denadai-Souza, A.; Stakenborg, N.; et al. Spatially Resolved Transcriptomic Profiling of Degraded and Challenging Fresh Frozen Samples. *Nat. Commun.* **2023**, *14* (1), 509.

(45) McKellar, D. W.; Mantri, M.; Hinchman, M. M.; Parker, J. S.; Sethupathy, P.; Cosgrove, B. D.; De Vlaminck, I. Spatial Mapping of the Total Transcriptome by in Situ Polyadenylation. *Nat. Biotechnol.* **2023**, *41* (4), 513−520.

(46) Lötstedt, B.; Stražar, M.; Xavier, R.; Regev, A.; Vickovic, S. Spatial Host−Microbiome Sequencing Reveals Niches in the Mouse Gut. *Nat. Biotechnol.* **2023**, DOI: 10.1038/s41587-023-01988-1.

(47) Saarenpää, S.; Shalev, O.; Ashkenazy, H.; Carlos, V.; Lundberg, D. S.; Weigel, D.; Giacomello, S. Spatial Metatranscriptomics Resolves Host−Bacteria−Fungi Interactomes. *Nat. Biotechnol.* **2023**, DOI: 10.1038/s41587-023-01979-2.

(48) Liu, Y.; Yang, M.; Deng, Y.; Su, G.; Enninful, A.; Guo, C. C.; Tebaldi, T.; Zhang, D.; Kim, D.; Bai, Z.; et al. High-Spatial-Resolution Multi-Omics Sequencing via Deterministic Barcoding in Tissue. *Cell* **2020**, *183* (6), 1665−1681.

(49) Zhang, D.; Deng, Y.; Kukanja, P.; Agirre, E.; Bartosovic, M.; Dong, M.; Ma, C.; Ma, S.; Su, G.; Bao, S.; Liu, Y.; Xiao, Y.; Rosoklija, G. B.; Dwork, A. J.; Mann, J. J.; Leong, K. W.; Boldrini, M.; Wang, L.; Haeussler, M.; Raphael, B. J.; Kluger, Y.; Castelo-Branco, G.; Fan, R. Spatial Epigenome−Transcriptome Co-Profiling of Mammalian Tissues. *Nature* **2023**, *616* (7955), 113−122.

(50) Russell, A. J. C.; Weir, J. A.; Nadaf, N. M.; Shabet, M.; Kumar, V.; Kambhampati, S.; Raichur, R.; Marrero, G. J.; Liu, S.; Balderrama, K. S.; Vanderburg, C. R.; Shanmugam, V.; Tian, L.; Iorgulescu, J. B.; Yoon, C. H.; Wu, C. J.; Macosko, E. Z.; Chen, F. Slide-Tags Enables Single-Nucleus Barcoding for Multimodal Spatial Genomics. *Nature* **2024**, *625*, 101.

(51) Zhao, T.; Chiang, Z. D.; Morriss, J. W.; LaFave, L. M.; Murray, E. M.; Del Priore, I.; Meli, K.; Lareau, C. A.; Nadaf, N. M.; Li, J.; et al. Spatial Genomics Enables Multi-Modal Study of Clonal Heterogeneity in Tissues. *Nature* **2022**, *601* (7891), 85−91.

(52) Jiang, F.; Zhou, X.; Qian, Y.; Zhu, M.; Wang, L.; Li, Z.; Shen, Q.; Wang, M.; Qu, F.; Cui, G.; et al. Simultaneous Profiling of Spatial Gene Expression and Chromatin Accessibility during Mouse Brain Development. *Nat. Methods* **2023**, *20*, 1048−1057.

(53) Liu, Y.; DiStasio, M.; Su, G.; Asashima, H.; Enninful, A.; Qin, X.; Deng, Y.; Nam, J.; Gao, F.; Bordignon, P.; et al. High-Plex Protein and Whole Transcriptome Co-Mapping at Cellular Resolution with Spatial CITE-Seq. *Nat. Biotechnol.* **2023**, *41*, 1405−1409.

(54) Deng, Y.; Bartosovic, M.; Kukanja, P.; Zhang, D.; Liu, Y.; Su, G.; Enninful, A.; Bai, Z.; Castelo-Branco, G.; Fan, R. Spatial-CUT&Tag: Spatially Resolved Chromatin Modification Profiling at Cellular Level. *Science* **2022**, *375* (6581), 681−686.

(55) Ben-Chetrit, N.; Niu, X.; Swett, A. D.; Sotelo, J.; Jiao, M. S.; Stewart, C. M.; Potenski, C.; Mielinis, P.; Roelli, P.; Stoeckius, M.; et al. Integration of Whole Transcriptome Spatial Profiling with Protein Markers. *Nat. Biotechnol.* **2023**, *41* (6), 788−793.

(56) Stoeckius, M.; Hafemeister, C.; Stephenson, W.; Houck-Loomis, B.; Chattopadhyay, P. K.; Swerdlow, H.; Satija, R.; Smibert, P. Simultaneous Epitope and Transcriptome Measurement in Single Cells. *Nat. Methods* **2017**, *14* (9), 865−868.

(57) Peterson, V. M.; Zhang, K. X.; Kumar, N.; Wong, J.; Li, L.; Wilson, D. C.; Moore, R.; McClanahan, T. K.; Sadekova, S.; Klappenbach, J. A. Multiplexed Quantification of Proteins and Transcripts in Single Cells. *Nat. Biotechnol.* **2017**, *35* (10), 936−939.

(58) Llorens-Bobadilla, E.; Zamboni, M.; Marklund, M.; Bhalla, N.; Chen, X.; Hartman, J.; Frisén, J.; Ståhl, P. L. Solid-Phase Capture and Profiling of Open Chromatin by Spatial ATAC. *Nat. Biotechnol.* **2023**, *41*, 1085−1088.

(59) Deng, Y.; Bartosovic, M.; Ma, S.; Zhang, D.; Kukanja, P.; Xiao, Y.; Su, G.; Liu, Y.; Qin, X.; Rosoklija, G. B.; Dwork, A. J.; Mann, J. J.; Xu, M. L.; Halene, S.; Craft, J. E.; Leong, K. W.; Boldrini, M.; Castelo-Branco, G.; Fan, R. Spatial Profiling of Chromatin Accessibility in Mouse and Human Tissues. *Nature* **2022**, *609* (7926), 375−383.

(60) Picelli, S.; Björklund, Å. K.; Reinius, B.; Sagasser, S.; Winberg, G.; Sandberg, R. Tn5 Transposase and Tagmentation Procedures for Massively Scaled Sequencing Projects. *Genome Res.* **2014**, *24* (12), 2033−2040.

(61) Kaya-Okur, H. S.; Wu, S. J.; Codomo, C. A.; Pledger, E. S.; Bryson, T. D.; Henikoff, J. G.; Ahmad, K.; Henikoff, S. CUT&Tag for Efficient Epigenomic Profiling of Small Samples and Single Cells. *Nat. Commun.* **2019**, *10* (1), 1930.

(62) Wirth, J.; Huber, N.; Yin, K.; Brood, S.; Chang, S.; Martinez-Jimenez, C. P.; Meier, M. Spatial Transcriptomics Using Multiplexed Deterministic Barcoding in Tissue. *Nat. Commun.* **2023**, *14* (1), 1523.

(63) Cao, J.; Zheng, Z.; Sun, D.; Chen, X.; Cheng, R.; Lv, T.; An, Y.; Zheng, J.; Song, J.; Wu, L.; et al. Decoder-Seq Enhances mRNA Capture Efficiency in Spatial RNA Sequencing. *Nat. Biotechnol.* **2024**, DOI: 10.1038/s41587-023-02086-y.

(64) Liu, Y.; Yang, M.; Deng, Y.; Su, G.; Enninful, A.; Guo, C. C.; Tebaldi, T.; Zhang, D.; Kim, D.; Bai, Z.; Norris, E.; Pan, A.; Li, J.; Xiao, Y.; Halene, S.; Fan, R. High-Spatial-Resolution Multi-Omics Sequencing via Deterministic Barcoding in Tissue. *Cell* **2020**, *183* (6), 1665−1681.e18.

(65) Rodriques, S. G.; Stickels, R. R.; Goeva, A.; Martin, C. A.; Murray, E.; Vanderburg, C. R.; Welch, J.; Chen, L. M.; Chen, F.; Macosko, E. Z. Slide-Seq: A Scalable Technology for Measuring Genome-Wide Expression at High Spatial Resolution. *Science* **2019**, *363* (6434), 1463−4167.

(66) Stickels, R. R.; Murray, E.; Kumar, P.; Li, J.; Marshall, J. L.; Di Bella, D. J.; Arlotta, P.; Macosko, E. Z.; Chen, F. Highly Sensitive Spatial Transcriptomics at Near-Cellular Resolution with Slide-seqV2. *Nat. Biotechnol.* **2021**, *39* (3), 313−319.

(67) Chen, A.; Liao, S.; Cheng, M.; Ma, K.; Wu, L.; Lai, Y.; Qiu, X.; Yang, J.; Xu, J.; Hao, S.; Wang, X.; Lu, H.; Chen, X.; Liu, X.; Huang, X.; Li, Z.; Hong, Y.; Jiang, Y.; Peng, J.; Liu, S.; Shen, M.; Liu, C.; Li, Q.; Yuan, Y.; Wei, X.; Zheng, H.; Feng, W.; Wang, Z.; Liu, Y.; Wang, Z.; Yang, Y.; Xiang, H.; Han, L.; Qin, B.; Guo, P.; Lai, G.; Muñoz-Cánoves, P.; Maxwell, P. H.; Thiery, J. P.; Wu, Q.-F.; Zhao, F.; Chen, B.; Li, M.; Dai, X.; Wang, S.; Kuang, H.; Hui, J.; Wang, L.; Fei, J.-F.; Wang, O.; Wei, X.; Lu, H.; Wang, B.; Liu, S.; Gu, Y.; Ni, M.; Zhang, W.; Mu, F.; Yin, Y.; Yang, H.; Lisby, M.; Cornall, R. J.; Mulder, J.; Uhlén, M.; Esteban, M. A.; Li, Y.; Liu, L.; Xu, X.; Wang, J. Spatiotemporal Transcriptomic Atlas of Mouse Organogenesis Using DNA Nanoball-Patterned Arrays. *Cell* **2022**, *185* (10), 1777−1792.e21.

(68) Cho, C.-S.; Xi, J.; Si, Y.; Park, S.-R.; Hsu, J.-E.; Kim, M.; Jun, G.; Kang, H. M.; Lee, J. H. Microscopic Examination of Spatial Transcriptome Using Seq-Scope. *Cell* **2021**, *184* (13), 3559−3572.e22.

(69) Fu, X.; Sun, L.; Dong, R.; Chen, J. Y.; Silakit, R.; Condon, L. F.; Lin, Y.; Lin, S.; Palmiter, R. D.; Gu, L. Polony Gels Enable Amplifiable DNA Stamping and Spatial Transcriptomics of Chronic Pain. *Cell* **2022**, *185* (24), 4621−4633.e17.

(70) Stickels, R. R.; Murray, E.; Kumar, P.; Li, J.; Marshall, J. L.; Di Bella, D. J.; Arlotta, P.; Macosko, E. Z.; Chen, F. Highly Sensitive Spatial Transcriptomics at Near-Cellular Resolution with Slide-seqV2. *Nat. Biotechnol.* **2021**, *39* (3), 313−319.

(71) Vickovic, S.; Eraslan, G.; Salmén, F.; Klughammer, J.; Stenbeck, L.; Schapiro, D.; Äijö, T.; Bonneau, R.; Bergenstråhle, L.; Navarro, J. F.; Gould, J.; Griffin, G. K.; Borg, Å.; Ronaghi, M.; Frisén, J.; Lundeberg, J.; Regev, A.; Ståhl, P. L. High-Definition Spatial Transcriptomics for in Situ Tissue Profiling. *Nat. Methods* **2019**, *16* (10), 987−990.

(72) Vahid, M. R.; Brown, E. L.; Steen, C. B.; Zhang, W.; Jeon, H. S.; Kang, M.; Gentles, A. J.; Newman, A. M. High-Resolution Alignment of Single-Cell and Spatial Transcriptomes with Cyto-SPACE. *Nat. Biotechnol.* **2023**, *41*, 1543−1548.

(73) Lee, Y.; Bogdanoff, D.; Wang, Y.; Hartoularos, G. C.; Woo, J. M.; Mowery, C. T.; Nisonoff, H. M.; Lee, D. S.; Sun, Y.; Lee, J.; et al. XYZeq: Spatially Resolved Single-Cell RNA Sequencing Reveals Expression Heterogeneity in the Tumor Microenvironment. *Sci. Adv.* **2021**, *7* (17), No. eabg4755.

(74) Srivatsan, S. R.; Regier, M. C.; Barkan, E.; Franks, J. M.; Packer, J. S.; Grosjean, P.; Duran, M.; Saxton, S.; Ladd, J. J.; Spielmann, M.; et al. Embryo-Scale, Single-Cell Spatial Transcriptomics. *Science* **2021**, *373* (6550), 111−117.

(75) Cao, J.; Packer, J. S.; Ramani, V.; Cusanovich, D. A.; Huynh, C.; Daza, R.; Qiu, X.; Lee, C.; Furlan, S. N.; Steemers, F. J.; et al. Comprehensive Single-Cell Transcriptional Profiling of a Multicellular Organism. *Science* **2017**, *357* (6352), 661−667.

(76) 10x Genomics. *Visium platform page*. https://www.10xgenomics.com/platforms/visium (accessed 2024-02-07).

(77) Lovatt, D.; Ruble, B. K.; Lee, J.; Dueck, H.; Kim, T. K.; Fisher, S.; Francis, C.; Spaethling, J. M.; Wolf, J. A.; Grady, M. S.; et al. Transcriptome in Vivo Analysis (TIVA) of Spatially Defined Single Cells in Live Tissue. *Nat. Methods* **2014**, *11* (2), 190−196.

(78) Salmen, F.; De Jonghe, J.; Kaminski, T. S.; Alemany, A.; Parada, G. E.; Verity-Legg, J.; Yanagida, A.; Kohler, T. N.; Battich, N.; Van Den Brekel, F.; Ellermann, A. L.; Arias, A. M.; Nichols, J.; Hemberg, M.; Hollfelder, F.; Van Oudenaarden, A. High-Throughput Total RNA Sequencing in Single Cells Using VASA-Seq. *Nat. Biotechnol.* **2022**, *40* (12), 1780−1793.

(79) Xu, Z.; Zhang, T.; Chen, H.; Zhu, Y.; Lv, Y.; Zhang, S.; Chen, J.; Chen, H.; Yang, L.; Jiang, W.; Ni, S.; Lu, F.; Wang, Z.; Yang, H.; Dong, L.; Chen, F.; Zhang, H.; Chen, Y.; Liu, J.; Zhang, D.; Fan, L.; Guo, G.; Wang, Y. High-Throughput Single Nucleus Total RNA Sequencing of Formalin-Fixed Paraffin-Embedded Tissues by snRandom-Seq. *Nat. Commun.* **2023**, *14* (1), 2734.

(80) Isakova, A.; Neff, N.; Quake, S. R. Single-Cell Quantification of a Broad RNA Spectrum Reveals Unique Noncoding Patterns Associated with Cell Types and States. *Proc. Natl. Acad. Sci. U. S. A.* **2021**, *118* (51), No. e2113568118.

(81) Engblom, C.; Thrane, K.; Lin, Q.; Andersson, A.; Toosi, H.; Chen, X.; Steiner, E.; Lu, C.; Mantovani, G.; Hagemann-Jensen, M.; Saarenpää, S.; Jangard, M.; Saez-Rodriguez, J.; Michaëlsson, J.; Hartman, J.; Lagergren, J.; Mold, J. E.; Lundeberg, J.; Frisén, J. Spatial Transcriptomics of B Cell and T Cell Receptors Reveals Lymphocyte Clonal Dynamics. *Science* **2023**, *382* (6675), No. eadf8486.

(82) Liu, S.; Iorgulescu, J. B.; Li, S.; Borji, M.; Barrera-Lopez, I. A.; Shanmugam, V.; Lyu, H.; Morriss, J. W.; Garcia, Z. N.; Murray, E.; et al. Spatial Maps of T Cell Receptors and Transcriptomes Reveal Distinct Immune Niches and Interactions in the Adaptive Immune Response. *Immunity* **2022**, *55* (10), 1940−1952.

(83) Klimas, A.; Gallagher, B. R.; Wijesekara, P.; Fekir, S.; DiBernardo, E. F.; Cheng, Z.; Stolz, D. B.; Cambi, F.; Watkins, S. C.; Brody, S. L.; Horani, A.; Barth, A. L.; Moore, C. I.; Ren, X.; Zhao, Y. Magnify Is a Universal Molecular Anchoring Strategy for Expansion Microscopy. *Nat. Biotechnol.* **2023**, *41* (6), 858−869.

(84) Lin, S.; Yin, K.; Zhang, Y.; Lin, F.; Chen, X.; Zeng, X.; Guo, X.; Zhang, H.; Song, J.; Yang, C.; et al. Well-TEMP-Seq as a Microwell-Based Strategy for Massively Parallel Profiling of Single-Cell Temporal RNA Dynamics. *Nat. Commun.* **2023**, *14* (1), 1272.